# Dipolar Heteronuclear Correlation Solid-State NMR Experiments Between Half-Integer Quadrupolar Nuclei: The Case of $^{11}$B-$^{17}$O

*Rick W. Dorn,[1,2] Alexander L. Paterson,[2†] Ivan Hung,[3] Peter L. Gor'kov,[3] Austin J. Thompson,[1] Aaron D. Sadow,[1] Zhehong Gan,[3] Aaron J. Rossini[1,2*]*

*[1]Iowa State University, Department of Chemistry, Ames, IA, USA, 50011.*

*[2]US Department of Energy, Ames Laboratory, Ames, IA, USA, 50011.*

*[3]National High Magnetic Field Laboratory (NHMFL), Tallahassee, FL, USA 32310.*

AUTHOR INFORMATION

**Corresponding Author**

*e-mail: arossini@iastate.edu, phone: 515-294-8952.

[†] Current address: *National Magnetic Resonance Facility at Madison, University of Wisconsin-Madison, Madison, WI, USA 53706*

**TOC Graphic.**

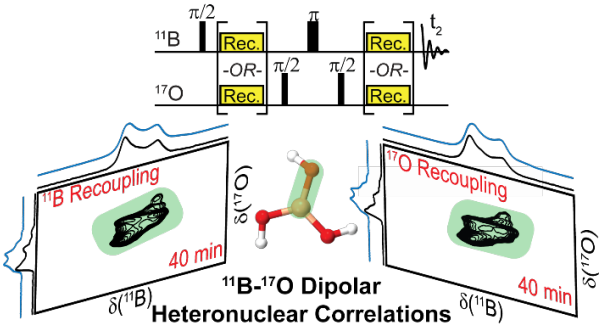


**Abstract.** With 73 % of all NMR-active nuclei being quadrupolar, there is great interest in the development of NMR experiments that can probe the proximity of quadrupolar spins. Here, pulse sequences for magic angle spinning (MAS) $^{11}$B-$^{17}$O Resonance-Echo Saturation-Pulse DOuble-Resonance (RESPDOR) and dipolar Heteronuclear Multiple Quantum Correlation (D-HMQC) solid-state NMR experiments were investigated. In these pulse sequences, Rotational-Echo Double-Resonance (REDOR) recoupling with central transition (CT) selective π-pulses were applied to either the $^{11}$B or $^{17}$O spins to recouple the $^{11}$B-$^{17}$O dipolar interactions. $^{11}$B{$^{17}$O} RESPDOR experiments on $^{17}$O-enriched boric acid and benzene diboronic acid showed that application of dipolar recoupling on the $^{11}$B channel yielded more signal dephasing than when recoupling is applied on the $^{17}$O channel; however, short effective $^{11}$B transverse relaxation time constants ($T_2$') hinders the acquisition of dephasing curves out to long recoupling durations. Application of REDOR recoupling to $^{17}$O spins was found to produce significant dephasing without compromising the $^{11}$B $T_2$'. Comparison of experimental $^{11}$B{$^{17}$O} RESPDOR curves to that of numerical simulations enabled the $^{17}$O isotopic enrichment to be estimated. 2D $^{11}$B{$^{17}$O} D-HMQC spectra were recorded with either $^{11}$B or $^{17}$O REDOR recoupling at a variety of radio frequency field conditions. Lastly, 2D $^{11}$B{$^{17}$O} and $^{23}$Na{$^{17}$O} D-HMQC spectra of a $^{17}$O-enriched sodium borate glass were acquired to demonstrate the practical application of these heteronuclear correlation experiments to probe structural connectivity between two quadrupolar

spins. Importantly, the high-field 2D $^{11}$B-$^{17}$O D-HMQC NMR spectrum revealed two unique $^{17}$O sites correlating to 4-coordinate $BO_4$ ($^{[4]}$B), which were attributed to the $^{[3]}$B-**O**-$^{[4]}$B and $^{[4]}$B-**O**-$^{[4]}$B bridging O atoms. The heteronuclear correlation experiments outlined here should be applicable to a variety of quadrupolar spin pairs.

**Introduction.**

High-resolution magic-angle spinning (MAS) solid-state NMR (SSNMR) spectroscopy is a powerful technique to determine molecular structure within crystalline and amorphous solids. Dipolar-based heteronuclear correlation (HETCOR) SSNMR experiments, such as Dipolar Heteronuclear Multiple-Quantum Correlation (D-HMQC), Transferred-Echo Double-Resonance (TEDOR) and Dipolar Refocused Insensitive Nuclei Enhanced through Polarization Transfer (D-RINEPT), are commonly used to probe through-space connectivity between two heteroatoms.[1-13] In MAS SSNMR spectroscopy, rotation of the sample about the magic angle (54.74°) with respect to the external magnetic field ($B_0$) will either partially or fully average the dipolar interaction between two dipolar-coupled spins. Therefore, heteronuclear dipolar recoupling techniques, such as Rotational-Echo Double-Resonance (REDOR),[2, 14-18] symmetry-based *C*-type (general formula: $CN_n^v$) and *R*-type (general formula: $RN_n^v$) sequences,[19-25] etc., are used to re-introduce the dipolar interaction during parts of the NMR experiment to enable through-space polarization transfer or to generate dipolar dephasing. Heteronuclear dipolar recoupling schemes are routinely applied to spin $I = 1/2$ nuclei to recouple interactions with other spin $I = 1/2$ or quadrupolar nuclei ($I > 1/2$).[6-7, 9, 11-12, 26-36]

SSNMR spectroscopy of quadrupolar nuclei is a growing field; approximately 73% of all NMR-active nuclei are quadrupolar, with the majority having half-integer spin (i.e., $I = 3/2$, 5/2,

7/2 or 9/2). Furthermore, many materials of interest that benefit from SSNMR structural characterization, such as metal-organic frameworks,[37-40] nanomaterials,[41-45] oxide glasses,[46-50] heterogenous catalysts[51-56] and pharmaceuticals,[11, 36, 57-64] contain abundant quadrupolar spins. Therefore, HETCOR NMR experiments between two quadrupolar nuclei could be useful to better elucidate chemical structure in many systems. Previously, $^{27}$Al-$^{17}$O 2D correlation SSNMR spectra were obtained by using HMQC experiments with coherence transfers mediated by scalar (*J*-) couplings.[65-68] Such experiments are essentially directly analogous to the $I = 1/2$ case because scalar couplings are not averaged by MAS and no radio frequency (RF) pulses are required during the *J*-evolution periods. *J*-based experiments are very powerful to determine molecular structure because they directly probe through-bond structural connectivity and have high theoretical efficiencies. For optimal efficiency, *J*-based experiments require one bond *J*-couplings ($^1J$) that are approximately larger than the inverse of the refocused transverse relaxation constant ($T_2$').[65] However, as shown here for $^{11}$B-$^{17}$O, dipolar-based experiments are much more efficient than *J*-based experiments because dipolar coupling constants are significantly larger than *J*-coupling constants (~ 2125 Hz compared to ~ 35 Hz, respectively) and $^{11}$B $T_2$' are much shorter than the inverse of $^1J$($^{11}$B-$^{17}$O).

Multiple groups have previously demonstrated that 2D dipolar-HETCOR NMR spectra between two half-integer quadrupolar spins can be recorded via cross-polarization (CP) under MAS conditions.[69-72] Unfortunately, spin-locking half-integer quadrupolar nuclei is often challenging and highly sample and site dependent.[73-74] Studies applying heteronuclear dipolar recoupling schemes to half-integer quadrupolar spins are relatively rare and have been primarily limited to obtain one-dimensional (1D) REDOR-type spectra.[46-48, 71, 75-78] To the best of our knowledge, there have only been two reports of 2D dipolar-based HETCOR NMR spectra

between two half-integer quadrupolar nuclei obtained by applying heteronuclear dipolar recoupling to one of the quadrupolar spins ($^{23}$Na-$^{27}$Al and $^{11}$B-$^{27}$Al).[79-80] In these examples, 2D $^{23}$Na{$^{27}$Al}/$^{27}$Al{$^{23}$Na} D-HMQC and D-RINEPT spectra were acquired with either Rotary Resonance Recoupling ($R^3$), $R2_1^1$ or $SR4$ applied to either the $^{23}$Na or $^{27}$Al spins,[79] while 2D $^{11}$B{$^{27}$Al}/$^{27}$Al{$^{11}$B} D-HMQC and D-RINEPT spectra were recorded with synchronous phase inversion $R^3$ (SPI-$R^3$; $C2_2^1$ symmetry) applied to either the $^{11}$B or $^{27}$Al spins.[80] Throughout this manuscript, the X{Y} notation indicates that the X spin is directly observed and the Y spin is indirectly detected.

In this contribution, we show that REDOR recoupling can be applied to either $^{11}$B ($I$ = 3/2) or $^{17}$O ($I$ = 5/2) to re-introduce the $^{11}$B-$^{17}$O dipolar interactions and allow $^{11}$B{$^{17}$O} Resonance-Echo Saturation-Pulse DOuble-Resonance (RESPDOR) and D-HMQC NMR experiments (Figure 1A and 1B, respectively). First, $^{11}$B{$^{17}$O} RESPDOR NMR experiments were used to confirm the successful re-introduction of the dipolar interaction and estimate the $^{17}$O-labeling percentages in $^{17}$O-enriched boric acid and benzene diboronic acid (BDBA). $^{11}$B{$^{17}$O} $J$-Resolved experiments were also performed to determine the 1-bond $^{11}$B-$^{17}$O $J$-coupling constants and estimate the $^{17}$O isotopic abundance. 2D $^{11}$B{$^{17}$O} D-HMQC NMR spectra were recorded by applying first-order $R^3$ or REDOR heteronuclear dipolar recoupling to either the $^{11}$B or $^{17}$O spins. Numerical simulations of $^{11}$B{$^{17}$O} D-HMQC suggest that the experiments are relatively robust to both the $^{11}$B and $^{17}$O quadrupolar coupling constant ($C_Q$) and also predict that the experiments operate with similar efficiencies at a variety of MAS frequencies ($\nu_{rot}$ = 10 – 50 kHz). Lastly, 2D $^{11}$B{$^{17}$O} and $^{23}$Na{$^{17}$O} D-HMQC spectra of a $^{17}$O-enriched sodium borate glass were acquired to demonstrate the practical utility of these heteronuclear correlation experiments to probe the structure of amorphous materials.

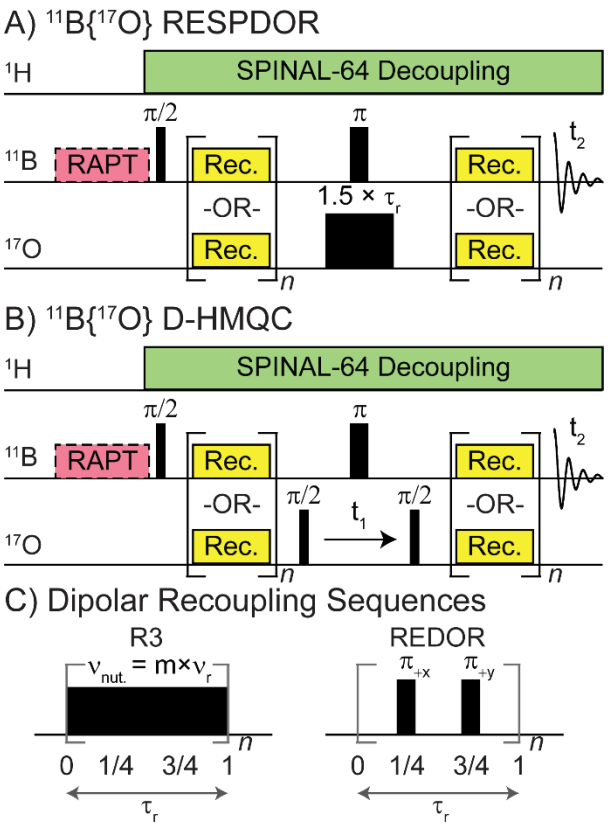


**Figure 1.** (A) $^{11}$B{$^{17}$O} RESPDOR and (B) $^{11}$B{$^{17}$O} D-HMQC NMR pulse sequences with (C) $R^3$ or REDOR heteronuclear dipolar recoupling (denoted Rec.) applied to either $^{11}$B or $^{17}$O.

**Methods.**

*Materials.* Benzene diboronic acid (BDBA, also referred as 1,4-phenyldiboronic acid; Oakwood Chemical – ACS Reagent) was $^{17}$O-enriched via recrystallization in 39.3 % $H_2{}^{17}O$ (Cortecnet). 45.1 mg of BDBA and 106.8 mg of 39.3 % $H_2{}^{17}O$ were mixed in a capped vial and heated to 70 °C in an oven for *ca.* 2 days. There was *ca.* 8 mg (corresponding to *ca.* 7 %) of $H_2{}^{17}O$ lost during the heating process. The vial was then placed in a Schlenk flask where excess water was removed at room temperature under a dynamic vacuum for *ca.* 1 day.

$^{17}$O-enriched boric acid was synthesized via the hydrolysis of borane ($BH_3$) with 39.3 % $^{17}$O-enriched $H_2O$ (Cortecnet). An oven-dried 50 mL round bottom Schlenk flask with a micro

stir bar was cooled under vacuum on a Schlenk line and then filled with $N_2$. The flask was charged with 1 M $BH_3$·THF solution (9.7 mL, 9.7 mmol; Sigma Aldrich) which was added by syringe under a $N_2$ purge. The $BH_3$·THF solution was cooled to −78 °C in a dry-ice/acetone bath for five min. 39.3 % $H_2{}^{17}O$ (0.59 mL, 31.1 mmol, 3.2 equiv.) was added dropwise by syringe over two min. Slight bubbling was observed. Upon full addition of the $H_2{}^{17}O$, the solution was allowed to stir for 30 min at −78 °C, then it was warmed to room temperature and stirred for 2 h. The volatiles were removed *in vaccuo* overnight to yield a white powder (0.607 g), which was used without further purification. The $^{17}O$-enrichment of boric acid was determined to be 30 % from solution $^{17}O$ NMR spectroscopy (see Supporting Information for more details).

A $^{17}O$-enriched sodium borate glass was synthesized with a composition of $41.5Na_2O$–$58.5B_2O_3$ (values given in mol %). Appropriately weighed amounts of sodium carbonate (99.999 % trace metals basis, Sigma-Aldrich) and 30 % $^{17}O$-enriched boric acid were mixed and thoroughly ground in a porcelain mortar and pestle. The mixed reagents were transferred to a 95/5 Pt/Au crucible which was topped with a Pt lid. The crucible and lid were placed in a 1050 °C furnace for approximately 40 minutes. The melt was quenched by dipping the bottom of the crucible in a room-temperature water bath. The resulting glass was clear, colorless and free of any observable bubbles. The glass was stored in a desiccator and was ground to a powder immediately before measurement by NMR spectroscopy.

*Solid-State NMR Spectroscopy at 9.4 T.* Solid-state NMR spectroscopy experiments were performed on a 9.4 T ($\nu_0(^1H)$ = 400 MHz) Bruker wide-bore magnet equipped with a Bruker Avance III HD console and a 2.5 mm triple-resonance MAS NMR probe. $^1H$ chemical shifts were referenced to 1% tetramethylsilane (TMS) in $CDCl_3$ by using solid adamantane ($\delta(^1H)$ = 1.71 ppm) as a secondary standard. $^{11}B$, $^{17}O$ and $^{23}Na$ shifts were indirectly referenced using the

previously published IUPAC recommended relative NMR frequencies.[81] The same shift referencing procedure was also used for 14.1 T NMR experiments. All NMR spectra were processed with the Bruker Topspin 3.6.1 software. 2D $^{11}$B MQMAS analytical simulations were performed with the ssNake NMR software.[82]

All experimental NMR parameters (magnetic field strength ($B_0$), MAS rate, recycle delay ($\tau_{\text{rec delay}}$), number of scans, $t_1$ TD points, $t_1$ dwell ($\Delta t_1$), $t_1$ acquisition time, dipolar recoupling duration and total experimental times) are given in Table S1. 2D $^{11}$B split-$t_1$ multiple-quantum MAS (MQMAS) experiments were performed with previously described pulse sequences.[83-86] The $^{11}$B 3Q excitation and 1Q reconversion pulse lengths were 3.45 μs and 0.98 μs in duration and applied at RF fields of *ca.* 186 kHz. 10 ° tip-angle single-pulse $^{11}$B NMR experiments were performed with a 0.833 μs pulse length, corresponding to a 8.3 kHz radio frequency (RF) field and 16.7 kHz central-transition (CT) nutation frequency. $^{23}$Na{$^{17}$O} D-HMQC experiments were performed with Rotor Assisted Population Transfer (RAPT) applied ± 250 kHz off resonance to the $^{23}$Na spins prior to the start of the experiment to enhance overall sensitivity.[87-88] $^{23}$Na CT-selective π/2 and π pulse lengths were 10 μs and 20 μs in duration, corresponding to a 12.5 kHz RF field and 25 kHz CT nutation frequency. The $^{17}$O CT-selective π/2 pulse length was 10 μs in duration, corresponding to a 8.3 kHz RF field and 25 kHz CT nutation frequency. 100 kHz $^{1}$H RF field of SPINAL-64 heteronuclear decoupling was performed throughout all NMR experiments.[89]

*Solid-State NMR Spectroscopy at 14.1 T.* Solid-state NMR spectroscopy experiments were performed on a 14.1 T ($\nu_0(^1\text{H})$ = 600 MHz) Bruker wide-bore magnet equipped with a Bruker NEO console and either a 4 mm triple resonance magic-angle spinning NMR probe ($^{11}$B{$^{17}$O} experiments) or a 2.5 mm triple-resonance MAS NMR probe configured in double

resonance mode ($^{17}$O MQMAS and $^{11}$B DQ-SQ experiments). The $^{1}$H, $^{11}$B and $^{17}$O channels of the 4 mm NMR probe were isolated with either bandpass ($^{1}$H and $^{11}$B) or lowpass ($^{17}$O) filters. All NMR spectra were processed with the Bruker Topspin 3.6.1 software. 2D $^{17}$O MQMAS analytical simulations were performed with the ssNake NMR software.[82]

The $^{11}$B CT-selective $\pi/2$ and $\pi$ pulse lengths were 15 μs and 30 μs in duration, corresponding to a 8.3 kHz RF field and 16.7 kHz CT nutation frequency. The $^{17}$O CT-selective $\pi/2$ and $\pi$ pulse lengths were 10 μs and 20 μs in duration, corresponding to a 8.3 kHz RF field and 25 kHz CT nutation frequency. 2D $^{11}$B{$^{17}$O} D-HMQC experiments were performed with our recently described Arbitrary Indirect Dwell (AID) $t_1$ acquisition mode and a 25 μs $t_1$ dwell.[90] Rotor Assisted Population Transfer (RAPT) was applied to the $^{11}$B spins with a transmitter offset of ± 550 kHz and a 10 kHz RF field prior to the start of NMR experiments.[87-88] $^{11}$B{$^{17}$O} RESPDOR experiments were performed with a 1.5 rotor period saturation pulse (150 μs for a 10 kHz MAS frequency) with a *ca.* 33 kHz $^{17}$O RF field. 2D $^{17}$O split-$t_1$ MQMAS experiments were performed with previously described pulse sequences.[83-85] The $^{17}$O 3Q excitation and 1Q reconversion pulse lengths were 5.75 μs and 1.25 μs in duration and applied at RF fields of *ca*. 68 kHz. A 2D $^{11}$B dipolar double-quantum-single-quantum (DQ-SQ) homonuclear correlation NMR spectrum of the $^{17}$O-enriched sodium borate glass was recorded with the $BR2_2^1$ homonuclear dipolar recoupling sequence.[91] A CT-selective $\pi$ pulse was applied during the $^{11}$B DQ $t_1$ evolution to ensure only CT DQ coherences between two $^{11}$B spins were observed.[92] Either 83.3 ($^{11}$B-$^{17}$O experiments) or 100 kHz ($^{11}$B DQSQ and $^{17}$O MQMAS) $^{1}$H RF field of SPINAL-64 heteronuclear decoupling was performed throughout all NMR experiments.[89]

*Solid-State NMR Spectroscopy at 18.8 T.* Solid-state NMR spectroscopy experiments were performed on an 18.8 T ($\nu_0$($^{1}$H) = 800 MHz) mid-bore magnet equipped with a Bruker

Avance III HD console and a 3.2 mm Low-E triple-resonance MAS NMR probe. $^{17}O$ chemical shifts were referenced to tap water ($\delta_{iso}$ = 2.83 ppm) with respect to $D_2O$ ($\delta_{iso}$ = 0.0 ppm). $^{11}B$ shifts were indirectly referenced using the previously published IUPAC recommended relative NMR frequency.[81] All NMR spectra were processed with the Bruker Topspin 3.6.1 software.

The $^{11}B$ CT-selective $\pi/2$ and $\pi$ pulse lengths were 6 μs and 12 μs in duration, corresponding to a 20.8 kHz RF field and 41.6 kHz CT nutation frequency. The $^{17}O$ CT-selective $\pi/2$ and $\pi$ pulse lengths were either 10 μs and 20 μs, or 15 μs and 30 μs in duration, corresponding to either a 8.3 or 5.6 kHz RF field and 25 or 16.7 kHz CT nutation frequency, respectively. 2D $^{11}B\{^{17}O\}$ D-HMQC experiments were performed with our recently described Arbitrary Indirect Dwell (AID) $t_1$ acquisition mode and either a (boric acid) 40 μs or (sodium borate glass) 12.5 μs $t_1$ dwell.[90] Rotor Assisted Population Transfer (RAPT) was applied to the $^{11}B$ spins with a transmitter offset of ± 500 kHz and either a 83.8 (boric acid) or 46.5 (borate glass) kHz RF field prior to the start of NMR experiments.[87-88] 100 kHz $^{1}H$ RF field SPINAL-64 heteronuclear decoupling was performed throughout all NMR experiments of boric acid.[89]

*Solid-State NMR Spectroscopy at 35.2 T.* 1D $^{11}B$ and $^{17}O$ NMR spectra were recorded at 35.2 T using a 36 T Series-Connected Hybrid (SCH) magnet (built and stationed at the National High Magnetic Field Laboratory in Tallahassee, FL) equipped with a Bruker Avance NEO console and a 2.0 mm HXY MAS NMR probe.[93] $^{11}B$ shifts were referenced to the $BO_4$ $^{11}B$ NMR signal observed at 18.8 T because the quadrupolar induce shift (QIS) is negligible when $C_Q < 0.5$ MHz at high field. $^{17}O$ shifts were indirectly referenced through $^{11}B$ shifts using the previously published IUPAC recommended relative $^{17}O$ NMR frequency.[81] All NMR spectra were recorded with a 20 kHz MAS frequency. Quantitative $^{11}B$ and $^{17}O$ NMR spectra were recorded with 15° or

30° single pulse experiment, respectively, and RF fields of 25 kHz (50 kHz $^{11}$B CT nutation frequency) or 8.3 kHz (25 kHz $^{17}$O CT nutation frequency), respectively.

*$^{11}$B-$^{17}$O RESPDOR, J-Resolved and D-HMQC Error Analysis.* Error bars were added to the experimental data points for all $^{11}$B-$^{17}$O RESPDOR and *J*-Resolved curves and the $^{11}$B{$^{17}$O} D-HMQC efficiencies to illustrate the level of uncertainty in the measurements. For all $^{11}$B{$^{17}$O} RESPDOR and *J*-Resolved curves, error bars are given by:

$$Error(\tau) = \frac{\sqrt{S_{0,norm} + S_{norm}} \times S_{0,1}}{2 \times SNR_{0,1} \times S_{0,norm}}$$

where $S_{0,norm}$ and $S_{norm}$ are the normalized control and dephased intensities for a given τ period (i.e., dipolar recoupling or *J*-evolution duration), $S_{0,1}$ ($S_{0,1} = 1$) is the control point that all control and dephased points are normalized to (i.e., maximum intensity, which will be the first time point), and $SNR_{0,1}$ is the signal-to-noise of the first control point (i.e., point $S_{0,1}$). $^{11}$B{$^{17}$O} D-HMQC efficiency error bars were determined based on the SNR of the 1D $^{11}$B{$^{17}$O} D-HMQC NMR spectrum:

$$Error = \frac{\sqrt{2}}{SNR} \times Efficency$$

2D $^{11}$B{$^{17}$O} D-HMQC integral error bars were determined based on the SNR of a $^{17}$O slice extracted at a frequency where the $^{11}$B signal intensity was largest:

$$Error = \frac{\sqrt{2}}{SNR} \times Integral$$

*Solid-State NMR Numerical Simulations.* Numerical solid-state NMR simulations of $^{11}$B{$^{17}$O} RESPDOR and D-HMQC experiments were performed using SIMPSON v4.2.1.[94-96] All simulations were performed at $B_0$ = 14.1 or 18.8 T with the rep168 crystal file, either (RESPDOR) 10 or (HMQC) 8 γ angles, and a 1 μs maximum time duration where the Hamiltonian was considered time independent. 2D heatplots of the $^{11}$B{$^{17}$O} D-HMQC

efficiency as a function of $^{11}$B and $^{17}$O $C_Q$ were obtained by running 2D SIMPSON simulations in which the $^{11}$B $C_Q$ was stepped from 0.5 – 4.5 MHz in steps of 0.25 MHz for each $^{17}$O $C_Q$ value (4 – 9 MHz, in steps of 0.25 MHz). The $^{11}$B and $^{17}$O isotropic shifts were updated for each individual simulation such that the $^{11}$B/$^{17}$O center of gravity peak position was at 0.0 ppm by calculating the quadrupolar induced shift for each $C_Q$ value. Two $^{11}$B-$^{17}$O D-HMQC SIMPSON simulations were performed for each $^{11}$B/$^{17}$O $C_Q$ value, where the phase of the second $^{17}$O $\pi/2$ pulse was incremented by 180°. The HMQC intensity for each $^{11}$B/$^{17}$O $C_Q$ value was obtained by subtracting the intensity of the HMQC recorded with a 180° phase inversion with the HMQC recorded with 0° phase and dividing the total signal by 2 (to account for addition of "two scans"). This phase cycling procedure was performed to obtain only the HMQC-filtered signal. The $^{11}$B{$^{17}$O} D-HMQC efficiency was then obtained by comparing the overall D-HMQC signal intensity to the signal intensity of an $^{11}$B spin echo with identical pulse parameters and spin-system parameters. The 2D heatplots were then constructed by importing the SIMPSON simulation output files into a matrix using MATLAB R2019a. 2D HMQC SIMPSON simulations used $^{11}$B and $^{17}$O Euler angles of boric acid that were obtained from plane-wave DFT calculations (*vide infra*, Figure S1). General 2D HMQC and RESPDOR SIMPSON input files, in addition to the MATLAB codes to generate the 2D heatplots, are available in the Supporting Information.

*Periodic Plane-Wave DFT Calculations.* The gauge-including projector-augmented wave (GIPAW)[97] approach as implemented in CASTEP version 2017 T2[98] was used for all periodic plane-wave density-functional theory (DFT) calculations. Only H atoms, if applicable, were geometry optimized while all other atomic coordinates were fixed to the positions determined from X-ray diffraction. Geometry optimizations of the H atom positions, when applicable, were

converged to an energy threshold of $5.0\times10^{-6}$ eV/atom, a maximum force threshold of 0.01 eV/Å and a maximum displacement threshold of $5.0\times10^{-4}$ Å, using the BFGS geometry optimization method.[99] All calculations utilized the Generalized Gradient Approximation (GGA) with the Perdew-Burke-Ernzerhof (PBE) exchange-correlation functional,[100] Tkatchenko-Scheffler (TS) dispersion corrections,[101] On-the-Fly ultrasoft Pseudopotentials (default settings in CASTEP),[102-103] zeroth-order regular approximation (ZORA) relativistic treatments,[104] a 0.07 $Å^{-1}$ k-point spacing and a 630 eV kinetic energy cutoff. Select DFT calculations were also performed with a 0.03 $Å^{-1}$ k-point spacing to confirm that the $^{17}O$ isotropic shieldings ($\sigma_{iso}$) converged with a 0.07 $Å^{-1}$ k-point spacing (the difference in shielding was between 0.00 and 0.04 ppm). DFT calculated $^{17}O$ $\sigma_{iso}$ were converted to $^{17}O$ isotropic chemical shifts ($\delta_{iso}$) via a previously published calibration plot utilizing identical DFT calculation parameters.[34] All crystal files (.cif) and NMR calculation output files (.magres) are available in the Supporting Information.

**Results/Discussion.**

*$^{11}B\{^{17}O\}$ RESPDOR.* $^{11}$B-$^{17}$O dipolar HETCOR SSNMR experiments were performed on BDBA and boric acid $^{17}$O-labeled to *ca.* 10 % (determined via $^{11}B\{^{17}O\}$ *J*-Resolved) and 30% (determined via solution $^{17}$O NMR), respectively, via either recrystallization in water (BDBA) or hydrolysis of $BH_3$ (boric acid). The $^{17}$O isotopic enrichment of the water used in synthesis was 39.3% in both cases. Molecular structures of boric acid and BDBA are shown in Figure S1. $^{11}B\{^{17}O\}$ RESPDOR NMR experiments were initially performed to confirm the successful re-introduction of the $^{11}$B-$^{17}$O dipolar interaction under MAS (Figure 1A and 1C). As mentioned above, REDOR type experiments have been performed for several quadrupolar nuclei combinations ($^{11}$B-$^{17}$O, $^{11}$B-$^{23}$Na, $^{11}$B-$^{27}$Al and $^{23}$Na-$^{51}$V).[46-48, 71, 75-78] We note that a RESPDOR experiment performed with REDOR dipolar recoupling is essentially the same as the Rotational-Echo Adiabatic-Passage DOuble-Resonance (REAPDOR) experiment introduced by Gullion and co-workers.[26-28, 30]

In a $^{11}B\{^{17}O\}$ RESPDOR experiment (Figure 1A) increasing the recoupling duration converts a larger fraction of in-phase $^{11}$B magnetization (e.g., $I_x$) to non-detectable, anti-phase $^{11}$B-$^{17}$O magnetization [e.g., $2I_yS_z\sin(\pi\kappa\omega_D\tau)$]. The anti-phase magnetization is not refocused when a saturation pulse is applied to the $^{17}$O spins, causing a loss of signal (dephasing). The rate at which the $^{11}$B NMR signal dephases is dependent on the strength of the dipolar coupling frequency which is proportional to the gyromagnetic ratio ($\gamma$) of both nuclei and the inverse cube of their inter-nuclear distance ($\omega_D \propto \frac{\gamma_i\gamma_j}{r_{ij}^3}$). Note that $\omega_D$ depends upon the orientation of the dipolar vector with respect to the external magnetic field. The requirement of generating anti-phase magnetization in a RESPDOR experiment serves as an ideal test if the dipolar interaction between two quadrupolar spins can be efficiently recoupled.

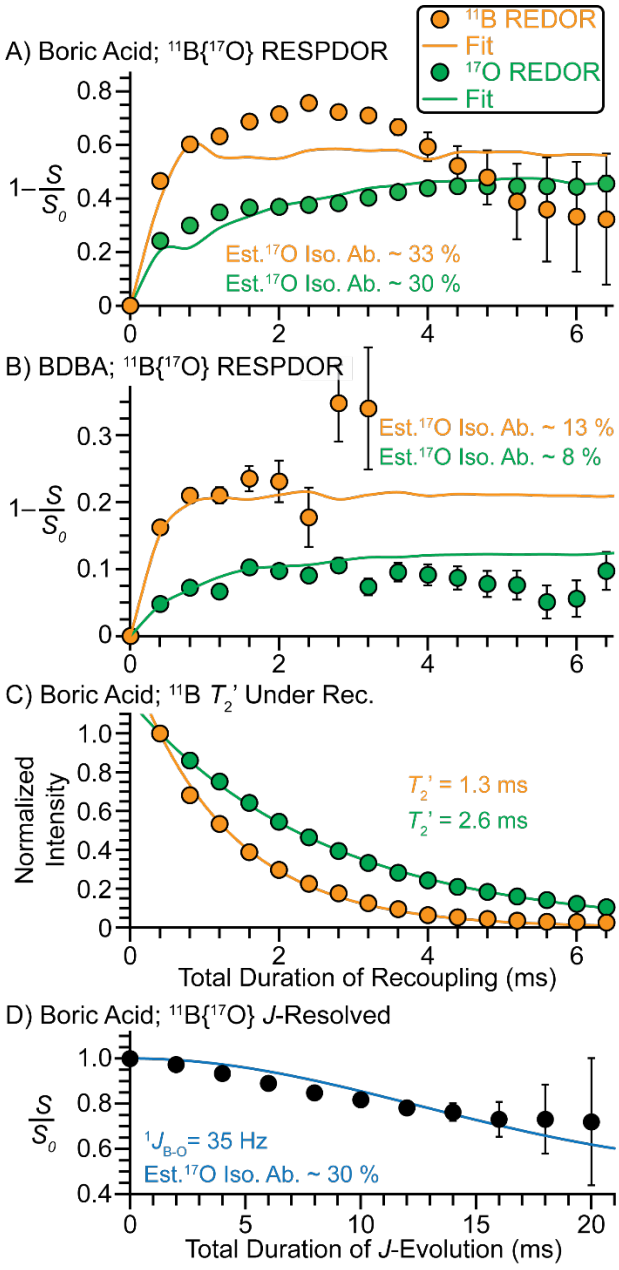


**Figure 2.** (A, B) $^{11}$B{$^{17}$O} RESPDOR curves of (A) boric acid and (B) BDBA recorded with either (green) 8.3 kHz RF field REDOR recoupling applied to the $^{17}$O spins or (orange) 6.25 kHz RF field REDOR recoupling applied to the $^{11}$B spins. (C) $^{11}$B $T_2$' measurement of boric acid under (orange) $^{11}$B (6.25 kHz RF field REDOR) or (green) $^{17}$O (8.3 kHz RF field REDOR) dipolar recoupling. (D) $^{11}$B{$^{17}$O} *J*-Resolved curve of boric acid recorded with a CT-selective $^{17}$O inversion ($\pi$) pulse. Experimental data points are shown as circles and (A-B) numerical simulations or (C-D) analytical fits are shown as solid lines. NMR experiments were performed at either (A, C-D) 18.8 T or (B) 14.1 T with a 10 kHz MAS frequency.

$^{11}$B{$^{17}$O} RESPDOR curves of boric acid and BDBA were recorded with either $B_0$ = 18.8 T or 14.1 T, respectively, and a 10 kHz MAS frequency (Figure 2A-B). REDOR heteronuclear dipolar recoupling was applied either to the $^{17}$O spins with a 8.3 kHz RF field (central transition (CT) nutation frequency = 25 kHz) or to the $^{11}$B spins with a 6.25 kHz RF field (CT nutation frequency = 12.5 kHz). The $^{11}$B{$^{17}$O} RESPDOR curves recorded with REDOR applied to the $^{11}$B spins yielded more signal dephasing and a faster build-up to maximum dephasing than when REDOR was applied to the $^{17}$O spins. The faster build-up to maximum dephasing when applying recoupling to the $^{11}$B spins is attributed to recoupling $^{11}$B CT spins to $^{17}$O spins residing in both CT spin states ($m_I = \pm 1/2$) and satellite transition (ST) spin states ($m_I = \pm 3/2, \pm 5/2$). In comparison, CT-selective REDOR recoupling $\pi$ pulses applied to $^{17}$O likely only recouples the $^{17}$O spins residing in CT states effectively, leading to a slower build-up and lower extent of dephasing. While applying recoupling to the observed $^{11}$B spins yields faster build-up and a higher extent of dephasing, the intensity of the control signal ($S_0$) more quickly reaches zero due to a decrease in the $^{11}$B $T_2$' (Figure 2C). Hence, the acquisition of curves out to longer durations of heteronuclear dipolar recoupling is challenging with $^{11}$B recoupling. In addition, when $^{11}$B REDOR recoupling is applied to boric acid the dephasing curve ($1 - S/S_0$) tends toward zero at longer durations of recoupling (Figure 2A, orange). The decrease in the dephasing curve observed at longer durations of recoupling likely arises because fluctuations in the experimental MAS frequency will result in improper refocusing of the $^{11}$B quadrupolar interaction and chemical shift anisotropy (CSA). $^{11}$B recoupling may also partially scramble the spins between all states/coherences and will also recouple $^{11}$B homonuclear dipolar couplings between CT and ST $^{11}$B spins. Consistent with our results Zheng and co-workers recently showed that the $T_2$' is significantly reduced when dipolar recoupling is applied to the directly detected channel in $^{11}$B-

$^{27}$Al D-HMQC experiments.[80] A similar trend in $^{11}$B $T_2$' was observed for BDBA (~ 5.5 ms under $^{17}$O recoupling and ~ 1.5 ms under $^{11}$B recoupling, Figure S2A).

Applying REDOR recoupling to the $^{17}$O spins enabled application of longer durations of heteronuclear dipolar recoupling without any clear decrease in the extent of dephasing at longer recoupling durations (Figure 2A, green). The observation that recoupling on the indirectly detected channel is more robust to MAS fluctuations is consistent with prior work from Garbow and Gullion, where they showed that π pulse mistiming of a few μs lead to significant intensity losses when applying REDOR recoupling to the observed spins.[105] In summary, based on the longer $^{11}$B $T_2$' and robustness to MAS fluctuations, application of REDOR recoupling to the indirectly detected spins (i.e., $^{17}$O) is generally preferred for RESPDOR type experiments.

*Measuring $^{17}$O Isotopic Enrichment*. From the X-ray crystal structures of BDBA and boric acid, it is known that a B-O bond length is *ca.* 1.35 Å.[106-107] Therefore, by scaling the intensity of two-spin (i.e. $^{11}$B-$^{17}$O) SIMPSON numerically simulated $^{11}$B{$^{17}$O} RESPDOR curves to match a B-O internuclear distance of 1.35 Å (dipolar coupling constant = 2125 Hz), the $^{17}$O-labeling percentage can be estimated. This is because the maximum dephasing of the $^{11}$B NMR signal is dependent on the $^{17}$O isotopic abundance (see Supporting Information for more discussion). Following this procedure, $^{17}$O-labeling percentages were determined with $^{11}$B{$^{17}$O} RESPDOR to be *ca.* 30 – 33% and 8 – 13% for boric acid and BDBA, respectively (Figure 2A-B). The estimated $^{17}$O isotopic enrichment of 30 – 33% determined for boric acid matches well to that determined from solution $^{17}$O NMR spectroscopy (~ 30%, Figure S3). We note that the experimental $^{11}$B{$^{17}$O} RESPDOR curves recorded with REDOR recoupling applied to the $^{11}$B spins shows higher than expected dephasing (before decreasing due to MAS fluctuations), which

is likely due to recoupling of intermolecular $^{11}$B-$^{17}$O spin pairs from nearby molecules within the crystal lattice.

The $^{17}$O isotopic abundance was also estimated via $^{11}$B{$^{17}$O} *J*-Resolved NMR experiments recorded with a CT-selective $^{17}$O inversion ($\pi$) pulse to selectively invert only the $^{17}$O CT (Figure 2D and S2B). Analytical fits that take into account the statistical probability of having an attached $^{17}$O atom residing in the CT spin state suggests that the $^{17}$O isotopic abundance of boric acid and BDBA is 30% and 10%, respectively, in excellent agreement with solution NMR and the $^{11}$B{$^{17}$O} RESPDOR results (see Supporting Information for *J*-Resolved fitting procedure). The 1-bond $^{11}$B-$^{17}$O *J*-coupling constants ($^1J_{BO}$) were determined to be 35 Hz, similar to that of B-O containing small molecules previously observed via solution NMR spectroscopy.[108] Euler angles used in the numerically simulated RESPDOR curves were obtained from periodic plane-wave DFT calculations of BDBA or boric acid (Figure S1), however, the Euler angles had a minimal effect on the simulated RESPDOR curves (Figure S4A). Numerical simulations also suggest that the rate and extent of signal dephasing in a $^{11}$B{$^{17}$O} RESPDOR experiment performed with $^{11}$B recoupling are nearly identical to that of a $^{13}$C{$^{17}$O} RESPDOR experiment with REDOR recoupling applied to the $^{13}$C spins, suggesting that both experiments exhibit similar mechanisms for dipolar recoupling, i.e., recoupling is driven by rotor-synchronized inversion or refocusing of the CT of the coupled or observed spin, respectively (Figure S4B).

*2D $^{11}$B{$^{17}$O} D-HMQC Experiments.* 2D $^{11}$B{$^{17}$O} D-HMQC NMR spectra of boric acid and BDBA were recorded at either $B_0$ = 14.1 or 18.8 T with a 10 kHz MAS frequency and first-order $R^3$ ($^{11}$B only) or REDOR heteronuclear dipolar recoupling applied to the $^{11}$B or $^{17}$O spins (Figure 3 and S5-10). Rotor Assisted Population Transfer (RAPT) was applied to the $^{11}$B spins at

the beginning of all HMQC experiments (Figure 1B).[87-88] We note that application of RAPT to the $^{17}$O spins concurrent with $^{11}$B recoupling could theoretically improve sensitivity and the rate of coherence build-up,[109-110] however, this strategy was not implemented here as the $^{17}$O channel of the NMR probe at 14.1 T exhibited a high *Q*, preventing efficient off-resonance $^{17}$O saturation.

2D $^{11}$B{$^{17}$O} D-HMQC spectra of boric acid (30 % $^{17}$O-enrichment, $^{11}$B $T_1$ ~ 7-10 s) were acquired in *ca.* 0.7 or 1.4 hours at $B_0$ = 18.8 or 14.1 T, respectively, while 2D $^{11}$B{$^{17}$O} D-HMQC spectra of BDBA (10 % $^{17}$O-enrichment, $^{11}$B $T_1$ ~ 10 s) were acquired in *ca.* 4 hours at $B_0$ = 14.1 T. All 2D $^{11}$B{$^{17}$O} D-HMQC spectra showed the expected correlations between $^{11}$B and $^{17}$O (Figure 3). The $^{11}$B projections extracted from the 2D HETCOR NMR spectra match relatively well to their ideal quadrupolar powder patterns, illustrating the ability to extract accurate $^{11}$B $C_Q$ and η values (Figure S11-13). The breadth of the extracted $^{17}$O projections matches well to the breadth of their ideal quadrupolar powder patterns, suggesting the magnitude the $^{17}$O $C_Q$ can be accurately determined. However, the shape of the extracted $^{17}$O projections all resemble that of η = 0, limiting the ability to accurately determine the $^{17}$O η from the 2D NMR spectra (Figures S11-13). We also recorded a 2D $^{11}$B{$^{17}$O} *J*-HMQC NMR spectrum of boric acid at $B_0$ = 18.8 T that reveals similarly distorted $^{11}$B and $^{17}$O projections, suggesting that the dipolar recoupling sequences are not necessarily the origin of the lineshape distortions (Figure S6D and S11). The 2D $^{11}$B{$^{17}$O} *J*-HMQC spectrum required a significantly longer acquisition time to acquire a spectrum with a similar signal-to-noise ratio as the 2D D-HMQC NMR spectra. All 2D $^{11}$B{$^{17}$O} D-HMQC spectra display a diagonal like contour pattern: $^{11}$B low frequency horn – $^{17}$O low frequency horn and $^{11}$B high frequency horn – $^{17}$O high frequency horn. In both boric acid and BDBA, planewave DFT calculations predict that the $V_{33}$ component of the $^{11}$B

EFG tensor is perpendicular to both the $^{11}$B-$^{17}$O dipole vector and $V_{33}$ component of the $^{17}$O EFG tensor (β Euler angle with respect to $^{11}$B EFG ~ 90 °).

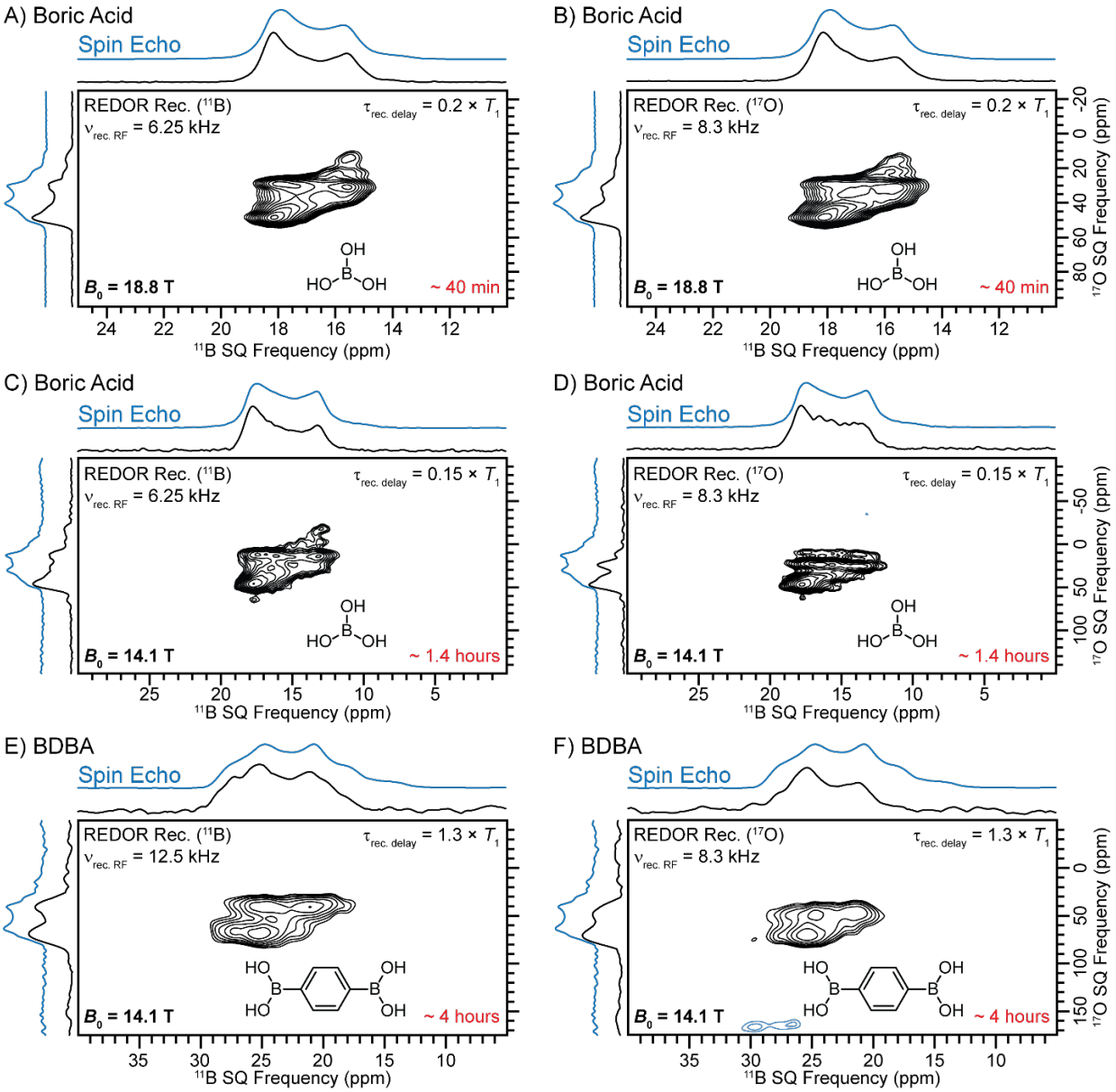


**Figure 3.** 2D $^{11}$B{$^{17}$O} D-HMQC spectra of (A – D) boric acid and (E, F) BDBA recorded at either (A-B) $B_0$ = 18.8 or (C-F) 14.1 T with a 10 kHz MAS frequency and 0.8 ms of total heteronuclear dipolar recoupling. The heteronuclear dipolar recoupling schemes, experimental times and recycle delays (relative to $T_1$) are listed within the NMR spectra. The 2D contour levels and spectral processing parameters within a set (i.e., A-B, C-D or D-F) are identical. $^{11}$B and $^{17}$O spin echo NMR spectra are displayed above the 2D projections. Molecular structures of boric acid and BDBA are shown within the NMR spectra.

The overall $^{11}B\{^{17}O\}$ D-HMQC NMR efficiencies were determined by comparing 1D HMQC spectra to that of an $^{11}B$ spin echo NMR spectrum where the total $^{11}B$ echo duration in both experiments were the same to account for $^{11}B$ $T_2$' relaxation (0.8 ms, Figure 4A-C and S14). Note that the $^{11}B$ $T_2$' is significantly shortened when REDOR recoupling is applied to the $^{11}B$ spins, further reducing the observed HMQC efficiencies (Figures 2C and S2A). For boric acid $^{11}B\{^{17}O\}$ D-HMQC efficiencies were *ca.* 1.7 – 6.3 % at $B_0$ = 14.1 or 18.8 T (Figure 4A-B). At 18.8 T, application of REDOR recoupling to the $^{17}O$ spins yielded the greatest HMQC efficiency (6.3 %), while at 14.1 T application of REDOR recoupling to the $^{11}B$ spins was most efficient (6.3 %). However, at both magnetic field strengths, the difference in HMQC efficiencies only varied by *ca.* 1 % between recoupling on the $^{11}B$ or $^{17}O$ channels. Numerical simulations (2 spin-system) of $^{11}B\{^{17}O\}$ D-HMQC with $^{11}B$ REDOR recoupling suggest an efficiency of *ca.* 10 % as compared to an $^{11}B$ spin echo, which is only slightly lower than that for $^{13}C\{^{17}O\}$ D-HMQC with $^{13}C$ REDOR recoupling (*ca.* 14 %, Figure S4C). Considering that the overall probability of having an attached $^{17}O$ to $^{11}B$ in 30 % $^{17}O$ enriched boric acid is ~ 66 %, the experimental $^{11}B\{^{17}O\}$ D-HMQC experiments are operating with similar efficiencies to those predicted by numerical SIMPSON simulations. Similar trends were observed for $^{11}B\{^{17}O\}$ D-HMQC experiments on BDBA (10 % $^{17}O$-enrichment) at $B_0$ = 14.1 T, where efficiencies were *ca.* 1.1 – 2.5 % (Figure 4C). The decrease in HMQC efficiency for BDBA as compared to boric acid is due to lower $^{17}O$ enrichment levels.

Signal integrations over the 2D contour plots were performed to better assess the relative D-HMQC efficiencies (Figure 4D-F). The trends in the 2D signal integrations with respect to the different recoupling sequences/conditions match near identically to the trends observed in the 1D $^{11}B\{^{17}O\}$ D-HMQC efficiencies. Importantly, the relative 2D signal integrations are similar

regardless of which spin REDOR recoupling was applied to. This observation is important because it implies that 2D D-HMQC experiments should be feasible for many different types of quadrupolar spin pairs.

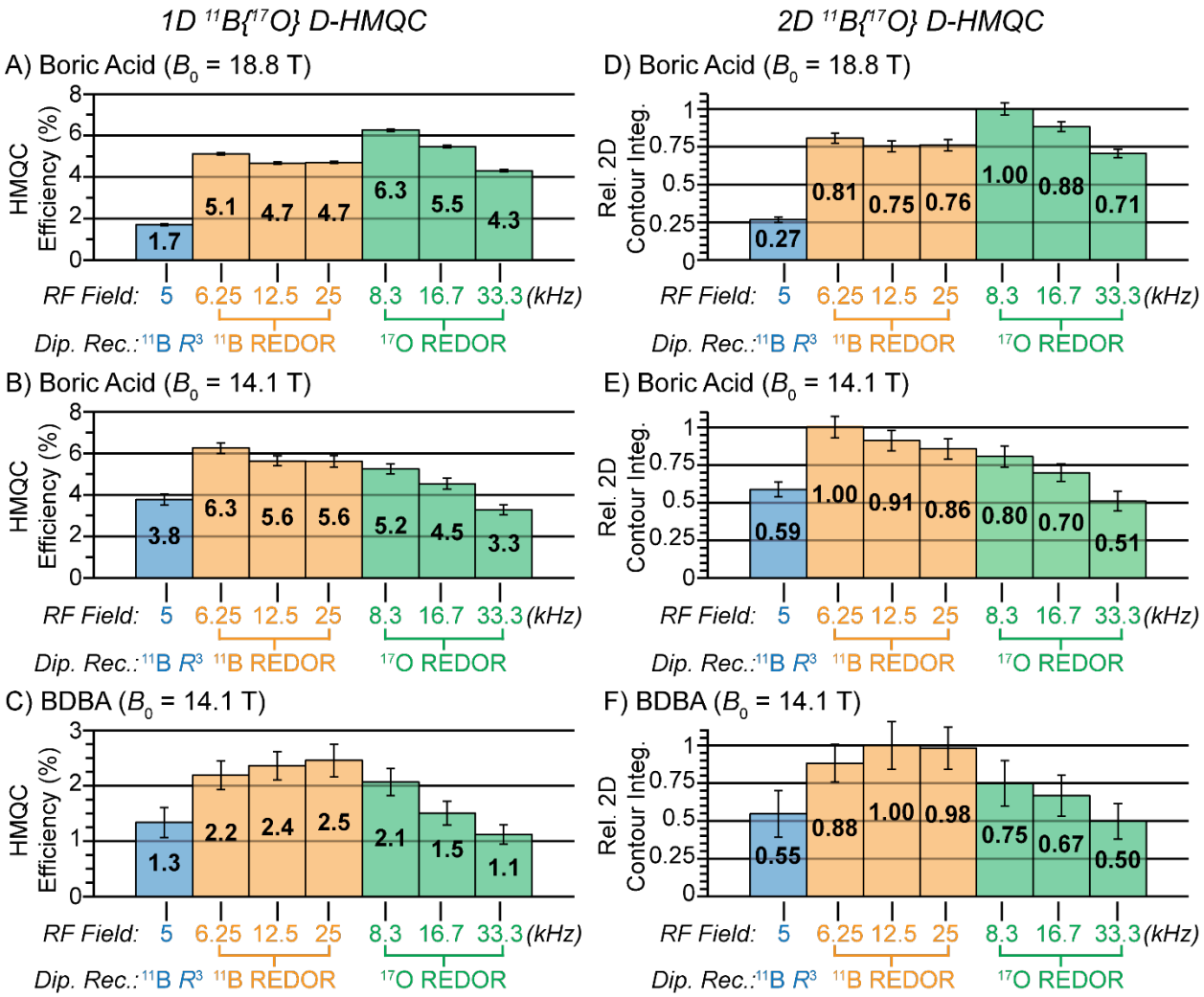


**Figure 4.** (A-C) Experimental $^{11}B\{^{17}O\}$ D-HMQC efficiencies for (A, B) boric acid and (C) BDBA. Efficiencies were determined by comparing 1D $^{11}B\{^{17}O\}$ D-HMQC NMR signal integrals to that of an $^{11}B$ spin echo spectrum. (D-F) Relative 2D $^{11}B\{^{17}O\}$ D-HMQC contour integrations for (D, E) boric acid and (F) BDBA. 1st order $R^3$ or REDOR heteronuclear dipolar recoupling schemes were applied to either the $^{11}B$ or $^{17}O$ spins ($^{11}B$ $R^3$ = blue, $^{11}B$ REDOR = orange, $^{17}O$ REDOR = green). NMR spectra were recorded at either (A, D) 18.8 T or (B-C, E-F) 14.1 T with a 10 kHz MAS frequency and 0.8 ms of total heteronuclear dipolar recoupling.

The effect that the $^{11}$B and $^{17}$O $C_Q$ have on the overall $^{11}$B{$^{17}$O} D-HMQC efficiencies was numerically investigated using the SIMPSON program.[94] Simulations of $^{11}$B{$^{17}$O} D-HMQC NMR experiments were performed with either 6.25 kHz, 12.5 kHz or 25 kHz RF field REDOR recoupling applied to the $^{11}$B spins, or 8.3 kHz, 16.7 kHz or 33.3 kHz RF field REDOR recoupling applied to the $^{17}$O spins (Figure 5). The 6.25 kHz RF field for $^{11}$B REDOR recoupling is essentially the lowest achievable RF field before the recoupling becomes $R^3$ (5 kHz RF field). Numerical simulations were performed at $B_0$ = 14.1 T with a 10 kHz MAS frequency and a two spin $^{11}$B-$^{17}$O spin system. $^{11}$B{$^{17}$O} D-HMQC efficiencies were determined by comparing numerically simulated $^{11}$B{$^{17}$O} D-HMQC to that of an $^{11}$B spin echo with the same spin system (Figure S15). We note that the $^{11}$B and $^{17}$O transmitters were placed on resonance with the center of gravity of each MAS powder pattern in all simulations (see *Methods*).

Comparison of the numerical simulations suggest that application of REDOR dipolar recoupling to the $^{11}$B spins is the most efficient recoupling scheme, in agreement with the experimental data discussed above (Figure 5). However, the numerical simulations do not account for $T_2$' relaxation, which explains why $^{17}$O recoupling offered similar efficiencies in the experiments. In general, the $^{11}$B{$^{17}$O} D-HMQC experiments are predicted to be relatively robust to both the $^{11}$B $C_Q$ (ranging from 0.5 – 4.5 MHz) and $^{17}$O $C_Q$ (ranging from 4.0 – 0.9 MHz). But, the overall HMQC signal intensity does decrease with increasing $^{17}$O $C_Q$. Some of the smaller $^{11}$B $C_Q$ values also show lower D-HMQC efficiency, likely because the $^{11}$B recoupling and spin echo p-pulses are no longer operating in the CT-selective regime. Additional $^{11}$B{$^{17}$O} D-HMQC numerical simulations were also performed with a 25 kHz or 50 kHz MAS frequency (Figure S16). Interestingly, the overall HMQC efficiency is predicted to increase at faster MAS frequencies when REDOR recoupling is applied to the $^{17}$O spins but is relatively constant at all

MAS frequencies under $^{11}$B recoupling. The prediction that $^{11}$B{$^{17}$O} D-HMQC experiments are feasible at a range of MAS frequencies further suggests the broad applicability of these experiments to a variety of systems. Lastly, we numerically investigated the effect that the offset of the REDOR recoupling pulses have on the overall $^{11}$B{$^{17}$O} D-HMQC efficiency for a variety of RF fields (Figure S17). As expected, the tolerance to offset increases with increasing RF field.

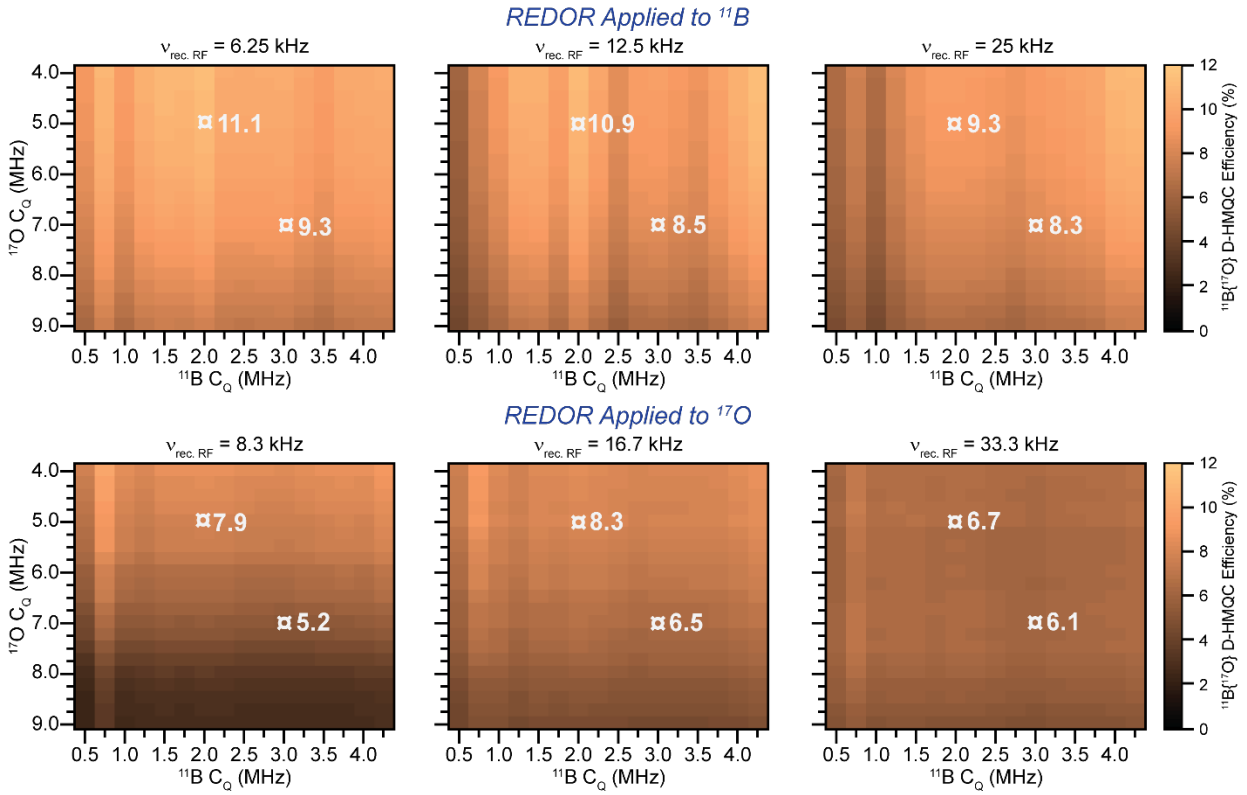


**Figure 5.** SIMPSON numerically simulated heat plots comparing the effects of $^{11}$B and $^{17}$O $C_Q$ on the overall $^{11}$B{$^{17}$O} D-HMQC efficiency under REDOR heteronuclear dipolar recoupling applied to either the (upper) $^{11}$B or (lower) $^{17}$O spins with the indicated RF fields. All simulations were performed at $B_0$ = 14.1 T with a 10 kHz MAS frequency and 0.8 ms of total heteronuclear dipolar recoupling. The white ¤ symbols indicate the $^{11}$B{$^{17}$O} D-HMQC efficiency for a given set of $^{11}$B and $^{17}$O $C_Q$ values.

*$^{17}$O-labeled Sodium Borate Glass.* The practical utility of the dipolar heteronuclear correlation experiments between two quadrupolar spins was demonstrated by recording 2D $^{11}$B{$^{17}$O} and $^{23}$Na{$^{17}$O} D-HMQC spectra of a $^{17}$O-labeled sodium borate glass with a composition of 41.5$Na_2O$–58.5$B_2O_3$ (amounts given in mol%). The $^{17}$O-enrichment of the glass

is estimated to be 15-20 % because 30 % $^{17}$O-enriched boric acid was used in the synthesis. An $^{11}$B MQMAS spectrum of the sodium borate glass shows two **B**O$_3$ ($^{[3]}$B) $^{11}$B NMR signals that were previously assigned to **B**(OB)$_3$ ($\delta_{iso}$ = 19.6 ppm, $C_Q$ = 2.6 MHz, $\eta$ = 0.3) and **B**(OB)$_x$(O$^-$)$_{2-x}$ ($\delta_{iso}$ = 18.5 ppm, $C_Q$ = 2.5 MHz, $\eta$ = 0.6) containing 1 or 2 non-bridging O atoms (Figure S18).[111-115] The observation that the site with a higher $\delta_{iso}$($^{11}$B) exhibits a lower $\eta$ is consistent with results previously reported by Stebbins and co-workers for a glass of similar composition.[111] There is also an intense, sharp $^{11}$B NMR signal near 0 ppm that can be assigned to **B**O$_4$ ($^{[4]}$B) species. 1D $^{11}$B NMR spectra recorded at $B_0$ = 9.4, 18.8 or 35.2 T further confirmed the identification of all $^{11}$B sites (Figure S17D).

Feller and co-workers previously described expressions for predicting the population of allowed borate units for different glass compositions; the glass composition is given by the parameter $R$ = mol% $Na_2O$/mol% $B_2O_3$.[116] $R$ = 0.71 for the 41.5$Na_2O$–58.5$B_2O_3$ sodium borate glass used in this study. Following their expression for the region of $0.7 \leq R < 1.0$, the sodium borate glass is predicted to contain 20 % triborate, 25 % metaborate, 30 % diborate and 25 % loose $BO_4$ units (Table 1, see *Supporting Information* for more details). The predicted population of $^{[4]}$B (45 %) is slightly higher than that determined experimentally (39 %). Consequently, the predicted population of metaborate units (25 %) is lower than that determined experimentally (40 %). Nevertheless, the experimentally determined populations of $^{[3]}$B and $^{[4]}$B (61 and 39 %, respectively) are in reasonable agreement with theoretical predictions (55 and 45 %, respectively).

**Table 1.** Predicted populations of borate units and experimentally determined populations of boron species in the sodium borate glass

| Borate Units | Labels | Predicted Populations (%)[a] | Boron Species | Experimentally Determined Populations (%)[b] |
|---|---|---|---|---|
| **Triborate** 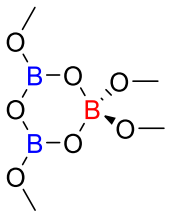 | $BO_3 = T^3$ | 15 | 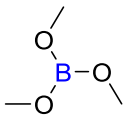 | 20 |
| | $BO_4 = T^4$ | 5 | | |
| **Metaborate** 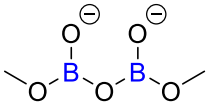 | $BO_3 = M^3$ | 25 | 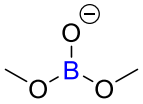 | 41 |
| **Diborate** 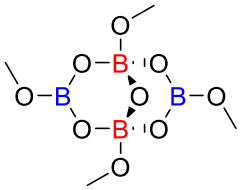 | $BO_3 = D^3$ | 15 | | |
| | $BO_4 = D^4$ | 15 | 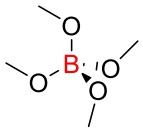 | 39 |
| **Loose $BO_4$** 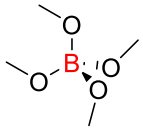 | $BO_4 = L^4$ | 25 | | |

[a] Populations were predicted based on the work of Feller *et al.* for $0.7 \leq R < 1.0$, where $R$ = mol% $Na_2O$/mol% $B_2O_3$.[116] [b] Determined from the quantitative $^{11}B$ NMR spectra.

Comparison of 1D $^{17}O$ direct excitation NMR spectra recorded at either $B_0$ = 14.1, 18.8 or 35.2 T with a 2D $^{17}O$ MQMAS spectrum recorded at $B_0$ = 14.1 T reveals two main groups of signals centered at *ca.* 57 ppm ($C_Q$ = 4.8 or 5.8 MHz) and 82 ppm in the 35.2 T spectrum ($C_Q$ = 4.8 MHz; Figure 6B and S19). Due to the significant CT quadrupolar line narrowing provided at 35.2 T, each group of $^{17}O$ NMR signals required two sites to analytically simulate the experimental 35.2 T $^{17}O$ NMR spectrum (Figure 6B, S19C and Table S2, see the *Supporting*

*Information* for more discussion). Previous 2D $^{17}$O MQMAS NMR spectra of a similar sodium borate glass identified two $^{17}$O NMR signals with isotropic shifts of *ca.* 56 ppm ($P_Q = C_Q\sqrt{1+\frac{\eta^2}{3}}$ = 5.6 MHz) and 82 ppm ($P_Q$ = 5.0 MHz) that were assigned to non-bridging B-**O**$^-$ and bridging B-**O**-B species, respectively.[111] We note that $^{17}$O SSNMR has been used to investigate other borate systems (sodium borate with more sodium, barium borate, crystalline $NaBO_2$), and in all cases, the bridging O atoms exhibit $^{17}$O isotropic chemical shifts greater than 80 ppm.[111] Specifically, for crystalline $NaBO_2$, bridging and non-bridging O atoms were determined to have isotropic chemical shifts of *ca.* 92 ppm and 80 ppm, respectively.[111]

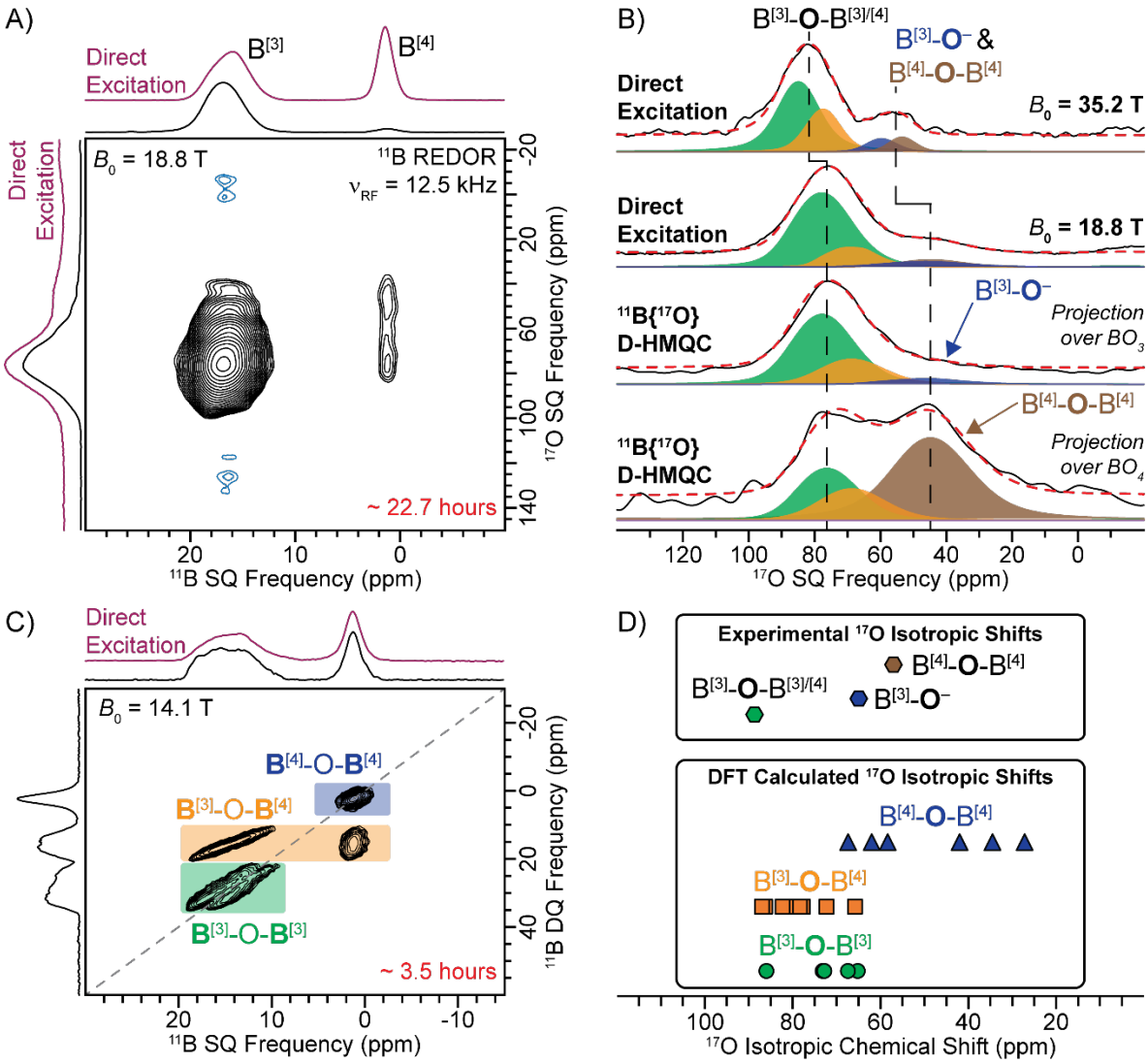


**Figure 6.** (A) 2D $^{11}B\{^{17}O\}$ D-HMQC spectrum of a $^{17}O$-enriched sodium borate glass recorded at $B_0$ = 18.8 T with a 10 kHz MAS frequency and 12.5 kHz RF field REDOR heteronuclear dipolar recoupling applied to the $^{11}B$ spins. (Purple) Direct excitation $^{11}B$ and $^{17}O$ NMR spectra are overlaid above the 2D projections. (B) Comparison of (upper) direct excitation $^{17}O$ NMR spectra ($B_0$ = 35.T or 18.8 T) to the $^{17}O$ NMR spectra obtained from projections from the 2D D-HMQC spectrum: (middle) projection over $^{[3]}B$ $^{11}B$ NMR signals (~ 22 – 12 ppm) and (lower) projection over $^{[4]}B$ $^{11}B$ NMR signals (~ 2 – 0 ppm). Experimental and analytically simulated spectra are shown as (solid) black and (dashed) red lines, respectively. (C) 2D $^{11}B$ dipolar double-quantum-single-quantum (DQ-SQ) homonuclear correlation NMR spectrum recorded at $B_0$ = 14.1 T with a 25 kHz MAS frequency and 320 μs of total $BR2_2^1$ homonuclear dipolar recoupling. (D) Comparison of (lower) periodic plane-wave DFT calculated $^{17}O$ isotropic chemical shifts of boron oxide-based materials with known crystal structures (Table S3) to that of (upper) $^{17}O$ isotropic chemical shifts of the sodium borate glass determined experimentally.

A 2D $^{11}B\{^{17}O\}$ D-HMQC NMR spectrum of the sodium borate glass was recorded at $B_0$ = 18.8 T with a 10 kHz MAS frequency and 12.5 kHz RF field REDOR recoupling applied to the $^{11}B$ spins (Figure 6A). This 2D NMR spectrum was acquired in just under 1 day, illustrating that HETCOR experiments between two quadrupolar spins should be feasible for a variety of materials. The 2D $^{11}B\{^{17}O\}$ D-HMQC spectrum displays multiple correlations between $^{17}O$ and $^{11}B$. The $^{[3]}B$ $^{11}B$ NMR signals centered at *ca.* 17 ppm mainly show correlations to $^{17}O$ NMR signals centered at *ca.* 75 ppm which were previously assigned to bridging O atoms ($^{[3]}B$-**O**-$^{[3]/[4]}B$; Figure 6B, projection over $^{[3]}B$). There are additional, weak correlations to the $^{17}O$ NMR signals centered at *ca.* 45 ppm that were previously assigned to non-bridging O atoms ($^{[3]}B$-$\mathbf{O}^-$; the center of the signal is much less than the isotropic chemical shift of 65 ppm due to quadrupolar signal broadening and the quadrupole induced shift). Interestingly, the $^{[4]}B$ $^{11}B$ NMR signal shows strong correlations to both $^{17}O$ NMR signals centered around 45 ppm and 75 ppm (Figure 6B, projection over $^{[4]}B$ ). The correlation between $^{[3]}B$ and the $^{17}O$ NMR signal centered at 75 ppm arises from $^{[3]}B$-**O**-$^{[4]}B$ units. The correlation of $^{[4]}B$ to the $^{17}O$ NMR signal centered at 45 ppm is intriguing. It is perhaps unexpected that $^{[4]}B$ contains a non-bridging O atom because the $^{[4]}B$ unit would then formally possess a net charge of –2. However, as discussed above, Feller and co-workers predicted abundant diborate species for this glass composition and the diborates contain a $^{[4]}B$-**O**-$^{[4]}B$ unit.

To further investigate the correlation between $^{[4]}B$ and the $^{17}O$ NMR signal centered at 45 ppm, we recorded a 2D $^{11}B$ dipolar double-quantum-single-quantum (DQ-SQ) homonuclear correlation NMR spectrum at $B_0$ = 14.1 T (Figure 6C). Intense $^{[4]}B$-$^{[4]}B$ homonuclear correlations were observed, implying that $^{[4]}B$ units linked via bridging O atoms must be common. Abundant $^{[4]}B$-O-$^{[4]}B$ motifs were recently identified in borosilicate glasses via $^{11}B$ DQ-SQ homonuclear

correlation NMR experiments.[117] Periodic plane-wave density-functional theory (DFT) NMR calculations of crystalline boron oxide-based system containing either $^{[3]}$B-**O**-$^{[3]}$B, $^{[3]}$B-**O**-$^{[4]}$B and/or $^{[4]}$B-**O**-$^{[4]}$B suggest that $^{[4]}$B-**O**-$^{[4]}$B bridging O atoms generally exhibit a lower $^{17}$O isotropic chemical shift as compared to $^{[3]}$B-**O**-$^{[3]}$B or $^{[3]}$B-**O**-$^{[4]}$B bridging O atoms (Figure 6D and Table S3). Therefore, we attribute the observed $^{11}$B-$^{17}$O heteronuclear correlations between $^{[4]}$B and the $^{17}$O NMR signals centered at 45 ppm to $^{[4]}$B-**O**-$^{[4]}$B units. As mentioned above, two O sites were required to analytically simulate the high resolution 35.2 T $^{17}$O NMR spectrum for the group of signals previously assigned to $^{[3]}$B-**O**$^{-}$ (centered at *ca.* 52 ppm at 35.2 T). Assuming $^{[4]}$B-**O**-$^{[4]}$B exhibits a similar $^{17}$O $C_Q$ as the other bridging O atoms ($^{[3]}$B-**O**-$^{[3]/[4]}$B, 4.8 MHz), the two sites likely correspond to $^{[3]}$B-**O**$^{-}$ (blue fit; $\delta_{iso}$ = 65 ppm and $C_Q$ = 5.8 MHz) and $^{[4]}$B-**O**-$^{[4]}$B (brown fit; $\delta_{iso}$ = 47 ppm and $C_Q$ = 4.8 MHz, Table S2). The $^{17}$O NMR signals of the $^{[3]}$B-**O**$^{-}$ and $^{[4]}$B-**O**-$^{[4]}$B sites are only partially resolved at 35.2 T and overlapping at lower magnetic fields (i.e., $B_0$ < 18.8 T). The population of each type of O atom was predicted by scaling the calculated population of the allowed borate units discussed above by the number of O atoms for each group (see *Supporting Information* for more discussion). This procedure predicts a glass containing 87 % $^{[3]}$B-**O**-$^{[3]/[4]}$B, 5 % $^{[4]}$B-**O**-$^{[4]}$B and 8 % $^{[3]}$B-**O**$^{-}$, in excellent agreement with populations determined from the fits of the 35.2 T $^{17}$O NMR spectrum (Table 2).

**Table 2.** Predicted and experimentally determined population of oxygen species in the sodium borate glass.

| Oxygen Species | Predicted Populations (%)[a] | Experimentally Determined Populations (%)[b] |
|---|---|---|
| $^{[3]}$B-**O**-$^{[3]/[4]}$B | 87 | 87 |
| $^{[4]}$B-**O**-$^{[4]}$B | 5 | 6 |
| $^{[3]}$B-**O**$^{-}$ | 8 | 7 |

[a] Populations were predicted by scaling the predicted boron unit populations in Table 1 by the number of oxygen atoms for a given group.[116] [b] Determined from fitting of the quantitative 35.2 T $^{17}$O NMR spectrum.

Lastly, a 2D $^{23}$Na{$^{17}$O} D-HMQC NMR spectrum was recorded at $B_0$ = 9.4 T with a 25 kHz MAS frequency and 16.7 kHz RF field REDOR applied to the $^{17}$O spins to illustrate the general applicability of these D-HMQC experiments to probe structural connectivity between two quadrupolar spins (Figure S20). All $^{17}$O NMR signals show correlations to $^{23}$Na. However, limited structural information can be obtained from the $^{23}$Na{$^{17}$O} D-HMQC spectrum due to the disordered nature of the glass and the low spectral resolution obtained at $B_0$ = 9.4 T.

## Conclusions

Here, we showed that application of REDOR heteronuclear dipolar recoupling to either the $^{11}$B or $^{17}$O spins can successfully re-introduce the $^{11}$B-$^{17}$O dipolar interaction in $^{11}$B{$^{17}$O} RESPDOR and D-HMQC solid-state NMR experiments. $^{11}$B{$^{17}$O} RESPDOR experiments were initially performed on boric acid and benzene diboronic acid (BDBA) $^{17}$O-labeled to *ca.* 30 % and 10 %, respectively. Application of REDOR recoupling to the $^{11}$B spins yielded more $^{11}$B signal dephasing than $^{17}$O recoupling, however, only a few points in the RESPDOR curve could be obtained due to short $^{11}$B $T_2$' under $^{11}$B recoupling. Therefore, $^{17}$O recoupling is more favorable for RESPDOR experiments as the $^{11}$B $T_2$' is significantly longer and thus more points at longer durations of recoupling could be obtained which better define the dipolar dephasing

build-up curve. Comparison of the experimental RESPDOR curves to that of numerical simulations of a two spin $^{11}$B-$^{17}$O spin system enabled an estimate of the $^{17}$O isotopic abundance. Following this method for boric acid, the $^{17}$O isotopic abundance was estimated to be 30-33 %, which matches well to the 30 % determined from solution NMR spectroscopy. We also recorded $^{11}$B{$^{17}$O} *J*-Resolved curves of boric acid and BDBA with CT-selective $^{17}$O inversions pulses to determine the 1-bond $^{11}$B-$^{17}$O *J*-coupling constants (~ 35 Hz) and estimate the $^{17}$O isotopic abundance.

2D $^{11}$B{$^{17}$O} D-HMQC spectra of boric acid and BDBA were recorded at either $B_0$ = 14.1 T or 18.8 T with REDOR recoupling applied to the $^{11}$B or $^{17}$O spins. In general, $^{11}$B REDOR recoupling performed better than $^{17}$O REDOR recoupling, however, $^{17}$O recoupling was favorable in some cases. The choice of the recoupling channel is likely sample and site dependent. The effect that the $^{11}$B and $^{17}$O $C_Q$ have on the overall D-HMQC efficiency was investigated with SIMPSON numerical simulations. At 10 kHz MAS, the D-HMQC efficiency was relatively robust to both the $^{11}$B and $^{17}$O $C_Q$ (0.5 – 4.5 MHz for $^{11}$B and 4.0 – 9.0 MHz for $^{17}$O). Interestingly, numerical simulations predicted that $^{11}$B{$^{17}$O} D-HMQC experiments operate at similar efficiencies at a variety of MAS frequencies (10 – 50 kHz). Lastly, we demonstrated the utility of using REDOR recoupling to enable HETCOR NMR experiments between two quadrupolar spins within materials by recording 2D $^{11}$B{$^{17}$O} and $^{23}$Na{$^{17}$O} D-HMQC spectra of a $^{17}$O-enriched sodium borate glass. The 2D $^{11}$B{$^{17}$O} D-HMQC spectrum revealed unexpected heteronuclear correlations between $^{[4]}$B and $^{17}$O NMR signals previously assigned to non-bridging O atoms. However, a 2D $^{11}$B dipolar DQ-SQ homonuclear correlation NMR spectrum revealed strong $^{[4]}$B-$^{[4]}$B homonuclear correlations, illustrating that $^{[4]}$B units linked via bridging O atoms must be common in this glass. Furthermore, periodic plane-wave DFT

calculations of boron oxide-based systems suggested that $^{[4]}$B-**O**-$^{[4]}$B bridging O atoms generally exhibit a lower $^{17}$O isotropic chemical shift as compared to $^{[3]}$B-**O**-$^{[3]}$B or $^{[3]}$B-**O**-$^{[4]}$B bridging O atoms. The heteronuclear correlations between $^{[4]}$B and lower frequency $^{17}$O NMR signals were assigned to $^{[4]}$B-**O**-$^{[4]}$B units. The $^{17}$O NMR signals for $^{[3]}$B-**O**$^{-}$ and $^{[4]}$B-**O**-$^{[4]}$B started to become slightly resolved at 35.2 T.

We anticipate that REDOR recoupling is generally applicable to an assortment of quadrupolar spins. The RESPDOR and D-HMQC experiments demonstrated here should be useful to study a variety of quadrupolar spin systems and materials.

## Supporting Information

The supporting information is available free of charge at XXX.

NMR experimental parameters, additional NMR spectra, discussion of $^{17}$O isotopic enrichment determination, SIMPSON numerical simulation files, MATLAB codes and CASTEP DFT calculated .cif and .magres files.

## Notes

The authors declare no competing financial interest. Raw NMR data, SIMPSON numerical simulation files, MATLAB codes, and CASTEP DFT calculated .cif and .magres files are available for download at DOI: 10.5281/zenodo.6376775

## Acknowledgements

This work was primarily supported by the National Science Foundation under Grant No. CBET-1916809. Borate glass synthesis (A.L.P.) was supported by the U.S. Department of

Energy (DOE), Office of Science, Basic Energy Sciences, Materials Science and Engineering Division. The Ames Laboratory is operated for the U.S. DOE by Iowa State University under Contract DE-AC02-07CH11358. Synthesis of $^{17}$O-labelled molecules (A.T. and A.D.S) was supported by the National Science Foundation under Grant No. CHE-1900393. A.J.R. acknowledges additional support from the Alfred P. Sloan Foundation through a Sloan research fellowship. This study made use of the National High Magnetic Field Laboratory to perform solid-state NMR spectroscopy experiments at high field. The National High Magnetic Field Laboratory is supported by the National Science Foundation through NSF/DMR-1644779 and the State of Florida. Development of the 36 T Series-Connected Hybrid (SCH) magnet and NMR instrumentation was supported by NSF (DMR-1039938 and DMR-0603042) and NIH P41 GM122698.

**References.**


1. Hing, A. W.; Vega, S.; Schaefer, J., Transferred-Echo Double-Resonance NMR. *J. Magn. Reson.* **1992,** *96* (1), 205-209.
2. Fyfe, C. A.; Mueller, K. T.; Grondey, H.; Wong-Moon, K. C., Dipolar Dephasing Between Quadrupolar and Spin-1/2 Nuclei. REDOR and TEDOR NMR Experiments on VPI-5. *Chem. Phys. Lett.* **1992,** *199* (1), 198-204.
3. Grey, C. P.; Veeman, W. S., The Detection of Weak Heteronuclear Coupling Between Spin 1 and Spin 1/2 Nuclei in MAS NMR; $^{14}N/^{13}C/^{1}H$ Triple Resonance Experiments. *Chem. Phys. Lett.* **1992,** *192* (4), 379-385.
4. Hing, A. W.; Vega, S.; Schaefer, J., Measurement of Heteronuclear Dipolar Coupling by Transferred-Echo Double-Resonance NMR. *J. Magn. Reson., Ser. A* **1993,** *103* (2), 151-162.
5. Grey, C. P.; Veeman, W. S.; Vega, A. J., Rotational echo $^{14}N/^{13}C/^{1}H$ triple resonance solid-state nuclear magnetic resonance: A probe of $^{13}C–^{14}N$ internuclear distances. *J. Chem. Phys.* **1993,** *98* (10), 7711-7724.
6. Trebosc, J.; Hu, B.; Amoureux, J. P.; Gan, Z., Through-Space R3-HETCOR Experiments Between Spin-1/2 and Half-Integer Quadrupolar Nuclei in Solid-State NMR. *J. Magn. Reson.* **2007,** *186* (2), 220-227.
7. Cavadini, S.; Abraham, A.; Bodenhausen, G., Proton-Detected Nitrogen-14 NMR by Recoupling of Heteronuclear Dipolar Interactions using Symmetry-Based Sequences. *Chem. Phys. Lett.* **2007,** *445* (1), 1-5.
8. Hu, B.; Trébosc, J.; Amoureux, J. P., Comparison of Several Hetero-Nuclear Dipolar Recoupling NMR Methods to be used in MAS HMQC/HSQC. *J. Magn. Reson.* **2008,** *192* (1), 112-122.
9. Lafon, O.; Wang, Q.; Hu, B.; Vasconcelos, F.; Trébosc, J.; Cristol, S.; Deng, F.; Amoureux, J.-P., Indirect Detection via Spin-1/2 Nuclei in Solid State NMR Spectroscopy: Application to the Observation of Proximities between Protons and Quadrupolar Nuclei. *J. Phys. Chem. A* **2009,** *113* (46), 12864-12878.
10. Martineau, C.; Bouchevreau, B.; Taulelle, F.; Trébosc, J.; Lafon, O.; Paul Amoureux, J., High-Resolution Through-Space Correlations Between Spin-1/2 and Half-Integer Quadrupolar Nuclei using the MQ-D-R-INEPT NMR Experiment. *Phys. Chem. Chem. Phys.* **2012,** *14* (19), 7112-7119.
11. Haimovich, A.; Goldbourt, A., Characterization of Lithium Coordination Sites with Magic-Angle Spinning NMR. *J. Magn. Reson.* **2015,** *254*, 131-138.
12. Venkatesh, A.; Hanrahan, M. P.; Rossini, A. J., Proton Detection of MAS Solid-State NMR Spectra of Half-Integer Quadrupolar Nuclei. *Solid State Nucl. Magn. Reson.* **2017,** *84*, 171-181.
13. Szeto, K. C.; Merle, N.; Trébosc, J.; Taoufik, M.; Gauvin, R. M.; Pourpoint, F.; Delevoye, L., Caveat on the Actual Robustness of Heteronuclear NMR Methods for Probing the Surface of γ-Alumina and Related Catalysts. *J. Phys. Chem. C* **2019,** *123* (20), 12919-12927.
14. Gullion, T.; Schaefer, J., Rotational-Echo Double-Resonance NMR. *J. Magn. Reson.* **1989,** *81* (1), 196-200.
15. Gullion, T.; Schaefer, J., Detection of Weak Heteronuclear Dipolar Coupling by Rotational-Echo Double-Resonance Nuclear Magnetic Resonance. In *Adv. Magn. Opt. Reson.*, Warren, W. S., Ed. Academic Press: 1989; Vol. 13, pp 57-83.

16. Schmidt, A.; McKay, R. A.; Schaefer, J., Internuclear Distance Measurement Between Deuterium (I = 1) and a Spin-1/2 Nucleus in Rotating Solids. *J. Magn. Reson.* **1992,** *96* (3), 644-650.
17. Gullion, T., Introduction to Rotational-Echo, Double-Resonance NMR. *Concepts Magn. Reson., Part A* **1998,** *10* (5), 277-289.
18. Bertmer, M.; Eckert, H., Dephasing of Spin Echoes by Multiple Heteronuclear Dipolar Interactions in Rotational Echo Double Resonance NMR Experiments. *Solid State Nucl. Magn. Reson.* **1999,** *15* (3), 139-152.
19. Lee, Y. K.; Kurur, N. D.; Helmle, M.; Johannessen, O. G.; Nielsen, N. C.; Levitt, M. H., Efficient Dipolar Recoupling in the NMR of Rotating Solids. A Sevenfold Symmetric Radiofrequency Pulse Sequence. *Chem. Phys. Lett.* **1995,** *242* (3), 304-309.
20. Hohwy, M.; Jakobsen, H. J.; Edén, M.; Levitt, M. H.; Nielsen, N. C., Broadband Dipolar Recoupling in the Nuclear Magnetic Resonance of Rotating Solids: A Compensated C7 Pulse Sequence. *J. Chem. Phys.* **1998,** *108* (7), 2686-2694.
21. Edén, M.; Levitt, M. H., Pulse Sequence Symmetries in the Nuclear Magnetic Resonance of Spinning Solids: Application to Heteronuclear Decoupling. *J. Chem. Phys.* **1999,** *111* (4), 1511-1519.
22. Carravetta, M.; Edén, M.; Zhao, X.; Brinkmann, A.; Levitt, M. H., Symmetry Principles for the Design of Radiofrequency Pulse Sequences in the Nuclear Magnetic Resonance of Rotating Solids. *Chem. Phys. Lett.* **2000,** *321* (3), 205-215.
23. Brinkmann, A.; Levitt, M. H., Symmetry Principles in the Nuclear Magnetic Resonance of Spinning Solids: Heteronuclear Recoupling by Generalized Hartmann–Hahn Sequences. *J. Chem. Phys.* **2001,** *115* (1), 357-384.
24. Zhao, X.; Edén, M.; Levitt, M. H., Recoupling of Heteronuclear Dipolar Interactions in Solid-State NMR using Symmetry-Based Pulse Sequences. *Chem. Phys. Lett.* **2001,** *342* (3), 353-361.
25. Levitt, M. H., Symmetry-Based Pulse Sequences in Magic-Angle Spinning Solid-State NMR. *eMagRes* **2007**.
26. Gullion, T., Measurement of Dipolar Interactions Between Spin-1/2 and Quadrupolar Nuclei by Rotational-Echo, Adiabatic-Passage, Double-Resonance NMR. *Chem. Phys. Lett.* **1995,** *246* (3), 325-330.
27. Chopin, L.; Vega, S.; Gullion, T., A MAS NMR Method for Measuring $^{13}C-^{17}O$ Distances. *J. Am. Chem. Soc.* **1998,** *120* (18), 4406-4409.
28. Hughes, E.; Gullion, T.; Goldbourt, A.; Vega, S.; Vega, A. J., Internuclear Distance Determination of S=1, I=1/2 Spin Pairs Using REAPDOR NMR. *J. Magn. Reson.* **2002,** *156* (2), 230-241.
29. Goldbourt, A.; Vega, S.; Gullion, T.; Vega, A. J., Interatomic Distance Measurement in Solid-State NMR between a Spin-1/2 and a Spin-5/2 Using a Universal REAPDOR Curve. *J. Am. Chem. Soc.* **2003,** *125* (37), 11194-11195.
30. Gullion, T.; Vega, A. J., Measuring Heteronuclear Dipolar Couplings for I=1/2, S>1/2 Spin Pairs by REDOR and REAPDOR NMR. *Prog. Nucl. Magn. Reson. Spectrosc.* **2005,** *47* (3), 123-136.
31. Brinkmann, A.; Kentgens, A. P. M., Proton-Selective $^{17}O-^{1}H$ Distance Measurements in Fast Magic-Angle-Spinning Solid-State NMR Spectroscopy for the Determination of Hydrogen Bond Lengths. *J. Am. Chem. Soc.* **2006,** *128* (46), 14758-14759.

32. Nimerovsky, E.; Goldbourt, A., Efficient Rotational Echo Double Resonance Recoupling of a Spin-1/2 and a Quadrupolar Spin at High Spinning Rates and Weak Irradiation Fields. *J. Magn. Reson.* **2010,** *206* (1), 52-58.
33. Nimerovsky, E.; Goldbourt, A., Distance Measurements Between Boron and Carbon at Natural Abundance using Magic Angle Spinning REAPDOR NMR and a Universal Curve. *Phys. Chem. Chem. Phys.* **2012,** *14* (38), 13437-13443.
34. Carnahan, S. L.; Lampkin, B. J.; Naik, P.; Hanrahan, M. P.; Slowing, I. I.; VanVeller, B.; Wu, G.; Rossini, A. J., Probing O–H Bonding through Proton Detected $^{1}H–^{17}O$ Double Resonance Solid-State NMR Spectroscopy. *J. Am. Chem. Soc.* **2019,** *141* (1), 441-450.
35. Duong, N. T.; Rossi, F.; Makrinich, M.; Goldbourt, A.; Chierotti, M. R.; Gobetto, R.; Nishiyama, Y., Accurate $^{1}H$-$^{14}N$ Distance Measurements by Phase-Modulated RESPDOR at Ultra-Fast MAS. *J. Magn. Reson.* **2019,** *308*, 106559.
36. Wijesekara, A. V.; Venkatesh, A.; Lampkin, B. J.; VanVeller, B.; Lubach, J. W.; Nagapudi, K.; Hung, I.; Gor'kov, P. L.; Gan, Z.; Rossini, A. J., Fast Acquisition of Proton-Detected HETCOR Solid-State NMR Spectra of Quadrupolar Nuclei and Rapid Measurement of NH Bond Lengths by Frequency Selective HMQC and RESPDOR Pulse Sequences. *Chem. - Eur. J.* **2020,** *26* (35), 7881-7888.
37. Martins, V.; Xu, J.; Wang, X.; Chen, K.; Hung, I.; Gan, Z.; Gervais, C.; Bonhomme, C.; Jiang, S.; Zheng, A., et al. Higher Magnetic Fields, Finer MOF Structural Information: $^{17}O$ Solid-State NMR at 35.2 T. *J. Am. Chem. Soc.* **2020,** *142*, 14877-14889.
38. Wang, W. D.; Lucier, B. E. G.; Terskikh, V. V.; Wang, W.; Huang, Y., Wobbling and Hopping: Studying Dynamics of $CO_2$ Adsorbed in Metal–Organic Frameworks via $^{17}O$ Solid-State NMR. *J. Phys. Chem. Lett.* **2014,** *5* (19), 3360-3365.
39. Sutrisno, A.; Huang, Y., Solid-Atate NMR: A Powerful Tool for Characterization of Metal–Organic Frameworks. *Solid State Nucl. Magn. Reson.* **2013,** *49-50*, 1-11.
40. Xu, J.; Blaakmeer, E. S. M.; Lipton, A. S.; McDonald, T. M.; Liu, Y. M.; Smit, B.; Long, J. R.; Kentgens, A. P. M.; Reimer, J. A., Uncovering the Local Magnesium Environment in the Metal–Organic Framework Mg2(dobpdc) Using $^{25}Mg$ NMR Spectroscopy. *J. Phys. Chem. C* **2017,** *121* (36), 19938-19945.
41. Dorn, R. W.; Ryan, M. J.; Kim, T.-H.; Goh, T. W.; Venkatesh, A.; Heintz, P. M.; Zhou, L.; Huang, W.; Rossini, A. J., Identifying the Molecular Edge Termination of Exfoliated Hexagonal Boron Nitride Nanosheets with Solid-State NMR Spectroscopy and Plane-Wave DFT Calculations. *Chem. Mater.* **2020,** *32* (7), 3109-3121.
42. Wang, M.; Wu, X.-P.; Zheng, S.; Zhao, L.; Li, L.; Shen, L.; Gao, Y.; Xue, N.; Guo, X.; Huang, W., et al. Identification of Different Oxygen Species in Oxide Nanostructures with $^{17}O$ Solid-State NMR Spectroscopy. *Sci. Adv.* **2015,** *1* (1), e1400133.
43. Zhang, W.; Bao, X.; Guo, X.; Wang, X., A High-Resolution Solid-State NMR Study on Nano-Structured HZSM-5 Zeolite. *Catal. Lett.* **1999,** *60* (1), 89-94.
44. Scolan, E.; Magnenet, C.; Massiot, D.; Sanchez, C., Surface and Bulk Characterisation of Titanium–Oxo Clusters and Nanosized Titania Particles Through $^{17}O$ Solid State NMR. *J. Mater. Chem.* **1999,** *9* (10), 2467-2474.
45. Etman, A. S.; Pell, A. J.; Svedlindh, P.; Hedin, N.; Zou, X.; Sun, J.; Bernin, D., Insights into the Exfoliation Process of $V_2O_5{\cdot}nH_2O$ Nanosheet Formation Using Real-Time $^{51}V$ NMR. *ACS Omega* **2019,** *4* (6), 10899-10905.

46. van Wüllen, L.; Züchner, L.; Müller-Warmuth, W.; Eckert, H., $^{11}B\{^{27}Al\}$ and $^{27}Al\{^{11}B\}$ Double Resonance Experiments on a Glassy Sodium Aluminoborate. *Solid State Nucl. Magn. Reson.* **1996,** *6* (3), 203-212.
47. Aguiar, P. M.; Michaelis, V. K.; McKinley, C. M.; Kroeker, S., Network Connectivity in Cesium Borosilicate Glasses: $^{17}O$ Multiple-Quantum MAS and Double-Resonance NMR. *J. Non-Cryst. Solids* **2013,** *363*, 50-56.
48. Funke, L. M.; Eckert, H., Charge Compensation in Sodium Borophosphate Glasses Studied by $^{11}B\{^{23}Na\}$ and $^{31}P\{^{23}Na\}$ Rotational Echo Double Resonance Spectroscopy. *J. Phys. Chem. C* **2016,** *120* (6), 3196-3205.
49. Paterson, A. L.; Hannon, A. C.; Werner-Zwanziger, U.; Zwanziger, J. W., Structural Differences between the Glass and Crystal Forms of the Transparent Ferroelectric Nanocomposite, $LaBGeO_5$, from Neutron Diffraction and NMR Spectroscopy. *J. Phys. Chem. C* **2018,** *122* (36), 20963-20980.
50. Eckert, H., Structural Characterization of Noncrystalline Solids and Glasses using Solid State NMR. *Prog. Nucl. Magn. Reson. Spectrosc.* **1992,** *24* (3), 159-293.
51. Wang, Q.; Li, W.; Hung, I.; Mentink-Vigier, F.; Wang, X.; Qi, G.; Wang, X.; Gan, Z.; Xu, J.; Deng, F., Mapping the Oxygen Structure of γ-$Al_2O_3$ by High-Field Solid-State NMR Spectroscopy. *Nat. Commun.* **2020,** *11* (1), 3620.
52. Ashbrook, S. E.; Smith, M. E., Solid State $^{17}O$ NMR—An Introduction to the Background Principles and Applications to Inorganic Materials. *Chem. Soc. Rev.* **2006,** *35* (8), 718-735.
53. Xu, J.; Wang, Q.; Deng, F., Metal Active Sites and Their Catalytic Functions in Zeolites: Insights from Solid-State NMR Spectroscopy. *Acc. Chem. Res.* **2019,** *52* (8), 2179-2189.
54. Love, A. M.; Cendejas, M. C.; Thomas, B.; McDermott, W. P.; Uchupalanun, P.; Kruszynski, C.; Burt, S. P.; Agbi, T.; Rossini, A. J.; Hermans, I., Synthesis and Characterization of Silica-Supported Boron Oxide Catalysts for the Oxidative Dehydrogenation of Propane. *J. Phys. Chem. C* **2019,** *123* (44), 27000-27011.
55. Chen, K.; Horstmeier, S.; Nguyen, V. T.; Wang, B.; Crossley, S. P.; Pham, T.; Gan, Z.; Hung, I.; White, J. L., Structure and Catalytic Characterization of a Second Framework Al(IV) Site in Zeolite Catalysts Revealed by NMR at 35.2 T. *J. Am. Chem. Soc.* **2020,** *142* (16), 7514-7523.
56. Dorn, R. W.; Cendejas, M. C.; Chen, K.; Hung, I.; Altvater, N. R.; McDermott, W. P.; Gan, Z.; Hermans, I.; Rossini, A. J., Structure Determination of Boron-Based Oxidative Dehydrogenation Heterogeneous Catalysts With Ultrahigh Field 35.2 T $^{11}B$ Solid-State NMR Spectroscopy. *ACS Catal.* **2020,** *10* (23), 13852-13866.
57. Hirsh, D. A.; Rossini, A. J.; Emsley, L.; Schurko, R. W., $^{35}Cl$ Dynamic Nuclear Polarization Solid-State NMR of Active Pharmaceutical Ingredients. *Phys. Chem. Chem. Phys.* **2016,** *18* (37), 25893-25904.
58. Hong, Y.-l.; Manjunatha Reddy, G. N.; Nishiyama, Y., Selective Detection of Active Pharmaceutical Ingredients in Tablet Formulations using Solid-State NMR Spectroscopy. *Solid State Nucl. Magn. Reson.* **2020,** *106*, 101651.
59. Pandey, M. K.; Kato, H.; Ishii, Y.; Nishiyama, Y., Two-Dimensional Proton-Detected $^{35}Cl/^{1}H$ Correlation Solid-State NMR Experiment Under Fast Magic Angle Sample Spinning: Application to Pharmaceutical Compounds. *Phys. Chem. Chem. Phys.* **2016,** *18* (8), 6209-6216.

60. Hamaed, H.; Pawlowski, J. M.; Cooper, B. F. T.; Fu, R.; Eichhorn, S. H.; Schurko, R. W., Application of Solid-State $^{35}$Cl NMR to the Structural Characterization of Hydrochloride Pharmaceuticals and their Polymorphs. *J. Am. Chem. Soc.* **2008,** *130* (33), 11056-11065.
61. Veinberg, S. L.; Johnston, K. E.; Jaroszewicz, M. J.; Kispal, B. M.; Mireault, C. R.; Kobayashi, T.; Pruski, M.; Schurko, R. W., Natural Abundance $^{14}$N and $^{15}$N Solid-State NMR of Pharmaceuticals and their Polymorphs. *Phys. Chem. Chem. Phys.* **2016,** *18* (26), 17713-17730.
62. Tatton, A. S.; Pham, T. N.; Vogt, F. G.; Iuga, D.; Edwards, A. J.; Brown, S. P., Probing Hydrogen Bonding in Cocrystals and Amorphous Dispersions Using $^{14}$N–$^{1}$H HMQC Solid-State NMR. *Mol. Pharmaceutics* **2013,** *10* (3), 999-1007.
63. Vogt, F. G.; Yin, H.; Forcino, R. G.; Wu, L., $^{17}$O Solid-State NMR as a Sensitive Probe of Hydrogen Bonding in Crystalline and Amorphous Solid Forms of Diflunisal. *Mol. Pharmaceutics* **2013,** *10* (9), 3433-3446.
64. Tatton, A. S.; Pham, T. N.; Vogt, F. G.; Iuga, D.; Edwards, A. J.; Brown, S. P., Probing Intermolecular Interactions and Nitrogen Protonation in Pharmaceuticals by Novel $^{15}$N-Edited and 2D $^{14}$N-$^{1}$H Solid-State NMR. *CrystEngComm* **2012,** *14* (8), 2654-2659.
65. Iuga, D.; Morais, C.; Gan, Z.; Neuville, D. R.; Cormier, L.; Massiot, D., NMR Heteronuclear Correlation between Quadrupolar Nuclei in Solids. *J. Am. Chem. Soc.* **2005,** *127* (33), 11540-11541.
66. Lee, S. K.; Deschamps, M.; Hiet, J.; Massiot, D.; Park, S. Y., Connectivity and Proximity between Quadrupolar Nuclides in Oxide Glasses: Insights from through-Bond and through-Space Correlations in Solid-State NMR. *J. Phys. Chem. B* **2009,** *113* (15), 5162-5167.
67. Chen, C.-H.; Gaillard, E.; Mentink-Vigier, F.; Chen, K.; Gan, Z.; Gaveau, P.; Rebière, B.; Berthelot, R.; Florian, P.; Bonhomme, C., et al. Direct $^{17}$O Isotopic Labeling of Oxides Using Mechanochemistry. *Inorg. Chem.* **2020,** *59*, 13050-13066.
68. Sukenaga, S.; Florian, P.; Kanehashi, K.; Shibata, H.; Saito, N.; Nakashima, K.; Massiot, D., Oxygen Speciation in Multicomponent Silicate Glasses Using Through Bond Double Resonance NMR Spectroscopy. *J. Phys. Chem. Lett.* **2017,** *8* (10), 2274-2279.
69. Chan, J. C. C.; Bertmer, M.; Eckert, H., Double-Quantum Cross-Polarization Between Half-Integer Quadrupolar Spin Systems: $^{11}$B↔$^{23}$Na and $^{11}$B↔$^{27}$Al. *Chem. Phys. Lett.* **1998,** *292* (1), 154-160.
70. Chan, J. C. C., High-Resolution Heteronuclear Correlation between Quadrupolar Nuclei. *J. Magn. Reson.* **1999,** *140* (2), 487-490.
71. Chan, J. C. C.; Bertmer, M.; Eckert, H., Site Connectivities in Amorphous Materials Studied by Double-Resonance NMR of Quadrupolar Nuclei: High-Resolution $^{11}$B ↔ $^{27}$Al Spectroscopy of Aluminoborate Glasses. *J. Am. Chem. Soc.* **1999,** *121* (22), 5238-5248.
72. Lu, X.; Tankamony, A. S. L.; Trébosc, J.; Lafon, O.; Amoureux, J.-P., Probing Proximities Between Different Quadrupolar Isotopes using Multi-Pulse Cross-Polarization. *J. Magn. Reson.* **2013,** *228*, 148-158.
73. Vega, A. J., CPMAS of Quadrupolar S = 3/2 Nuclei. *Solid State Nucl. Magn. Reson.* **1992,** *1* (1), 17-32.
74. Vega, A. J., MAS NMR Spin Locking of Half-Integer Quadrupolar Nuclei. *J. Magn. Reson.* **1992,** *96* (1), 50-68.
75. van Wüllen, L., Double Resonance Experiments in a Single Resonance Probe: Detecting $^{23}$Na–$^{51}$V Dipolar Interactions in Sodium Vanadates. *Solid State Nucl. Magn. Reson.* **1998,** *10* (4), 235-240.

76. Janssen, M.; Eckert, H., $^{11}B\{^{23}Na\}$ Rotational Ccho Double Resonance NMR: A New Approach for Studying the Spatial Cation Distribution in Sodium Borate Glasses. *Solid State Ionics* **2000,** *136-137*, 1007-1014.
77. Yang, J.; Zheng, A.; Zhang, M.; Luo, Q.; Yue, Y.; Ye, C.; Lu, X.; Deng, F., Brönsted and Lewis Acidity of the $BF_3/\gamma$-$Al_2O_3$ Alkylation Catalyst as Revealed by Solid-State NMR Spectroscopy and DFT Quantum Chemical Calculations. *J. Phys. Chem. B* **2005,** *109* (27), 13124-13131.
78. Hansen, M. R.; Jakobsen, H. J.; Skibsted, J., Structural Environments for Boron and Aluminum in Alumina−Boria Catalysts and Their Precursors from $^{11}B$ and $^{27}Al$ Single- and Double-Resonance MAS NMR Experiments. *J. Phys. Chem. C* **2008,** *112* (18), 7210-7222.
79. Xin, S.; Wang, Q.; Xu, J.; Feng, N.; Li, W.; Deng, F., Heteronuclear Correlation Experiments of $^{23}Na$-$^{27}Al$ in Rotating Solids. *Solid State Nucl. Magn. Reson.* **2017,** *84*, 103-110.
80. Zheng, M.; Xin, S.; Wang, Q.; Trébosc, J.; Xu, J.; Qi, G.; Feng, N.; Lafon, O.; Deng, F., Through-Space $^{11}B$–$^{27}Al$ Correlation: Influence of the Recoupling Channel. *Magn. Reson. Chem.* **2021,** *59* (9-10), 1062-1076.
81. Harris, R. K.; Becker, E. D.; Cabral de Menezes, S. M.; Goodfellow, R.; Granger, P., NMR Nomenclature: Nuclear Spin Properties and Conventions for Chemical Shifts: IUPAC Recommendations 2001. *Solid State Nucl. Magn. Reson.* **2002,** *22* (4), 458-483.
82. van Meerten, S. G. J.; Franssen, W. M. J.; Kentgens, A. P. M., ssNake: A Cross-Platform Open-Source NMR Data Processing and Fitting Application. *J. Magn. Reson.* **2019,** *301*, 56-66.
83. Frydman, L.; Harwood, J. S., Isotropic Spectra of Half-Integer Quadrupolar Spins from Bidimensional Magic-Angle Spinning NMR. *J. Am. Chem. Soc.* **1995,** *117* (19), 5367-5368.
84. Medek, A.; Harwood, J. S.; Frydman, L., Multiple-Quantum Magic-Angle Spinning NMR: A New Method for the Study of Quadrupolar Nuclei in Solids. *J. Am. Chem. Soc.* **1995,** *117* (51), 12779-12787.
85. Brown, S. P.; Wimperis, S., Two-Dimensional Multiple-Quantum MAS NMR of Quadrupolar Nuclei. Acquisition of the Whole Echo. *J. Magn. Reson.* **1997,** *124* (1), 279-285.
86. Hwang, S. J.; Fernandez, C.; Amoureux, J. P.; Cho, J.; Martin, S. W.; Pruski, M., Quantitative Study of the Short Range Order in $B_2O_3$ and $B_2S_3$ by MAS and Two-Dimensional Triple-Quantum MAS $^{11}B$ NMR. *Solid State Nucl. Magn. Reson.* **1997,** *8* (2), 109-121.
87. Yao, Z.; Kwak, H.-T.; Sakellariou, D.; Emsley, L.; Grandinetti, P. J., Sensitivity Enhancement of the Central Transition NMR Signal of Quadrupolar Nuclei under Magic-Angle Spinning. *Chem. Phys. Lett.* **2000,** *327* (1), 85-90.
88. Kwak, H.-T.; Prasad, S.; Clark, T.; Grandinetti, P. J., Enhancing Sensitivity of Quadrupolar Nuclei in Solid-State NMR with Multiple Rotor Assisted Population Transfers. *Solid State Nucl. Magn. Reson.* **2003,** *24* (2), 71-77.
89. Fung, B. M.; Khitrin, A. K.; Ermolaev, K., An Improved Broadband Decoupling Sequence for Liquid Crystals and Solids. *J. Magn. Reson.* **2000,** *142* (1), 97-101.
90. Venkatesh, A.; Perras, F. A.; Rossini, A. J., Proton-Detected Solid-State NMR Spectroscopy of Spin-1/2 Nuclei with Large Chemical Shift Anisotropy. *J. Magn. Reson.* **2021,** *327*, 106983.
91. Wang, Q.; Hu, B.; Lafon, O.; Trébosc, J.; Deng, F.; Amoureux, J. P., Double-Quantum Homonuclear NMR Correlation Spectroscopy of Quadrupolar Nuclei Subjected to Magic-Angle Spinning and High Magnetic Field. *J. Magn. Reson.* **2009,** *200* (2), 251-260.

92. Mali, G.; Fink, G.; Taulelle, F., Double-Quantum Homonuclear Correlation Magic Angle Sample Spinning Nuclear Magnetic Resonance Spectroscopy of Dipolar-Coupled Quadrupolar Nuclei. *J. Chem. Phys.* **2004,** *120* (6), 2835-2845.
93. Gan, Z.; Hung, I.; Wang, X.; Paulino, J.; Wu, G.; Litvak, I. M.; Gor'kov, P. L.; Brey, W. W.; Lendi, P.; Schiano, J. L., et al NMR Spectroscopy up to 35.2T using a Series-Connected Hybrid Magnet. *J. Magn. Reson.* **2017,** *284*, 125-136.
94. Bak, M.; Rasmussen, J. T.; Nielsen, N. C., SIMPSON: A General Simulation Program for Solid-State NMR Spectroscopy. *J. Magn. Reson.* **2000,** *147* (2), 296-330.
95. Tošner, Z.; Vosegaard, T.; Kehlet, C.; Khaneja, N.; Glaser, S. J.; Nielsen, N. C., Optimal Control in NMR Spectroscopy: Numerical Implementation in SIMPSON. *J. Magn. Reson.* **2009,** *197* (2), 120-134.
96. Tošner, Z.; Andersen, R.; Stevensson, B.; Edén, M.; Nielsen, N. C.; Vosegaard, T., Computer-Intensive Simulation of Solid-State NMR Experiments using SIMPSON. *J. Magn. Reson.* **2014,** *246*, 79-93.
97. Pickard, C. J.; Mauri, F., All-Electron Magnetic Response with Pseudopotentials: NMR Chemical Shifts. *Phys. Rev. B* **2001,** *63* (24), 245101.
98. Clark, S. J.; Segall, M. D.; Pickard, C. J.; Hasnip, P. J.; Probert, M. I. J.; Refson, K.; Payne, M. C., First Principles Methods using CASTEP. *Z. Kristallogr. - Cryst. Mater.* **2005,** *220* (5-6), 567-570.
99. Pfrommer, B. G.; Côté, M.; Louie, S. G.; Cohen, M. L., Relaxation of Crystals with the Quasi-Newton Method. *J. Comput. Phys.* **1997,** *131* (1), 233-240.
100. Perdew, J. P.; Burke, K.; Ernzerhof, M., Generalized Gradient Approximation Made Simple. *Phys. Rev. Lett.* **1996,** *77* (18), 3865-3868.
101. Tkatchenko, A.; Scheffler, M., Accurate Molecular Van Der Waals Interactions from Ground-State Electron Density and Free-Atom Reference Data. *Phys. Rev. Lett.* **2009,** *102* (7), 073005.
102. Vanderbilt, D., Soft Self-Consistent Pseudopotentials in a Generalized Eigenvalue Formalism. *Phys. Rev. B* **1990,** *41* (11), 7892-7895.
103. Yates, J. R.; Pickard, C. J.; Mauri, F., Calculation of NMR Chemical Shifts for Extended Systems using Ultrasoft Pseudopotentials. *Phys. Rev. B* **2007,** *76* (2), 024401.
104. Green, T. F. G.; Yates, J. R., Relativistic Nuclear Magnetic Resonance J-coupling with Ultrasoft Pseudopotentials and the Zeroth-Order Regular Approximation. *J. Chem. Phys.* **2014,** *140* (23), 234106.
105. Garbow, J. R.; Gullion, T., The Importance of Precise Timing in Pulsed, Rotor-Synchronous MAS NMR. *Chem. Phys. Lett.* **1992,** *192* (1), 71-76.
106. Shuvalov, R. R.; Burns, P. C., A New Polytype of Orthoboric Acid, $H_3BO_3$-3T. *Acta Crystallogr., Sect. C* **2003,** *59* (6), i47-i49.
107. Rodriguez-Cuamatzi, P.; Vargas-Diaz, G.; Maris, T.; Wuest, J. D.; Hopfl, H., 1,4-Phenylenediboronic Acid. *Acta Crystallogr., Sect. E* **2004,** *60* (8), o1316-o1318.
108. Wrackmeyer, B.; Tok, O. L., Indirect Nuclear Spin-Spin Coupling Constants $^{1}J(^{17}O,^{11}B)$. First Observation and Calculation using Density Functional Theory (DFT). *Z. Naturforsch., B* **2006,** *61* (8), 949-955.
109. Wang, Q.; Trébosc, J.; Li, Y.; Xu, J.; Hu, B.; Feng, N.; Chen, Q.; Lafon, O.; Amoureux, J.-P.; Deng, F., Signal enhancement of J-HMQC experiments in solid-state NMR involving half-integer quadrupolar nuclei. *Chem. Commun.* **2013,** *49* (59), 6653-6655.

110. Wang, Q.; Li, Y.; Trébosc, J.; Lafon, O.; Xu, J.; Hu, B.; Feng, N.; Chen, Q.; Amoureux, J.-P.; Deng, F., Population Transfer HMQC for Half-Integer Quadrupolar Nuclei. *J. Chem. Phys.* **2015,** *142* (9), 094201.
111. Stebbins, J. F.; Zhao, P.; Kroeker, S., Non-Bridging Oxygens in Borate Glasses: Characterization by $^{11}B$ and $^{17}O$ MAS and 3QMAS NMR. *Solid State Nucl. Magn. Reson.* **2000,** *16* (1), 9-19.
112. Kriz, H. M.; Bray, P. J., The $^{11}B$ Quadrupole Interaction and Nonbridging Oxygens in Crystalline Borates. *J. Magn. Reson.* **1971,** *4* (1), 76-84.
113. Kriz, H. M.; Bishop, S. G.; Bray, P. J., $^{11}B$ NMR in Polycrystalline Calcium Metaborate. *J. Chem. Phys.* **1968,** *49* (2), 557-561.
114. Kroeker, S.; Stebbins, J. F., Three-Coordinated Boron-11 Chemical Shifts in Borates. *Inorg. Chem.* **2001,** *40* (24), 6239-6246.
115. Aguiar, P. M.; Kroeker, S., Boron Speciation and Non-Bridging Oxygens in High-Alkali Borate Glasses. *J. Non-Cryst. Solids* **2007,** *353* (18), 1834-1839.
116. Feller, S. A.; Dell, W. J.; Bray, P. J., $^{10}B$ NMR studies of lithium borate glasses. *J. Non-Cryst. Solids* **1982,** *51* (1), 21-30.
117. Yu, Y.; Stevensson, B.; Edén, M., Direct Experimental Evidence for Abundant $BO_4$–$BO_4$ Motifs in Borosilicate Glasses From Double-Quantum $^{11}B$ NMR Spectroscopy. *J. Phys. Chem. Lett.* **2018,** *9* (21), 6372-6376.